Energy Reports 15 (2026) 109231

Contents lists available at ScienceDirect

Energy Reports

journal homepage: www.elsevier.com/locate/egyr

Research paper

A robust multi-stage FOPI(1+PID*n*) controller for precision control of switched reluctance motors under nonlinear and uncertain conditions

Mostafa Jabari [a], Serdar Ekinci [b], Davut Izci [c,d], Mohit Bajaj [e,f,g,*], Vojtech Blazek [h], Lukas Prokop [h]

[a] Faculty of Electrical Engineering, Sahand University of Technology, Tabriz, Iran
[b] Department of Computer Engineering, Bitlis Eren University, Bitlis, Turkey
[c] Department of Electrical and Electronics Engineering, Bursa Uludag University, Bursa 16059, Turkey
[d] Applied Science Research Center, Applied Science Private University, Amman 11937, Jordan
[e] Department of Electrical Engineering, Graphic Era (Deemed to be University), Dehradun 248002, India
[f] Hourani Center for Applied Scientific Research, Al-Ahliyya Amman University, Amman, Jordan
[g] Graphic Era Hill University, Dehradun 248002, India
[h] ENET Centre, CEET, VSB-Technical University of Ostrava, Ostrava 708 00, Czech Republic

ARTICLE INFO

Keywords:
Controller optimization
Dynamic response
FOPI controller
FOPI(1+PIDn)
Nonlinear systems
PSO-TVAC
Speed regulation
Switched reluctance motor
Torque ripple minimization
Uncertain conditions

ABSTRACT

Switched reluctance motors (SRMs) are recognized for their robustness, simplicity, and cost-effectiveness, yet they face inherent challenges in precise speed regulation and torque ripple minimization due to their doubly salient structure and nonlinear magnetic characteristics. This study introduces a novel and high-performance FOPI(1+PID*n*) multi-stage controller, specifically designed to address these critical limitations. The proposed control strategy synergistically integrates a fractional order proportional integral (FOPI) controller in the primary stage to enhance stability and transient response, with a proportional integral derivative controller augmented with a derivative filter (PID*n*) in the subsequent stage to improve dynamic adaptability and noise rejection. To achieve optimal tuning of controller parameters, a particle swarm optimization with time-varying acceleration coefficients (PSO-TVAC) is employed, using a robust cost function that simultaneously minimizes speed and current errors over simulation time. The effectiveness of the FOPI(1+PID*n*) controller is rigorously validated through extensive simulations in MATLAB/Simulink under a range of adverse conditions: no-load, static and dynamic loads, time-delay-induced nonlinearity, stepwise load increments, and parameter uncertainties for sensitivity analysis. Comparative assessments against conventional PID, PID*n*, and FOPID controllers demonstrate that the proposed controller consistently achieves superior performance, with an average improvement exceeding 45% across key dynamic response metrics including rise time, settling time, overshoot, and torque ripple. Notably, the proposed controller exhibits a 57% reduction in the cost function, a 65% reduction in integral of squared error (ISE), and enhanced robustness under uncertainty, establishing its efficacy for real-time control applications in SRMs. This work advances the state-of-the-art by offering a simple yet powerful control architecture that fuses classical and modern optimization techniques to deliver ultra-fast speed tracking, significant torque ripple attenuation, and strong resilience against nonlinear disturbances, thus broadening the operational viability of SRMs in precision-demanding industrial applications.

1. Introduction

Electric motors are widely used in both homes and industries (Gan et al., 2018). Among them, the switched reluctance motor (SRM) has gained much attention because of its strong design, low cost, and simple construction. It does not need permanent magnets or rotor windings, which makes it suitable for high-speed and high-temperature operation (Bogusz et al., 2021; Gengaraj et al., 2023; Souza et al., 2021). Because of these features, SRMs are often used as a cheaper alternative to induction motors (IMs) and permanent-magnet motors (PMMs) (Bogusz et al., 2021; Cai et al., 2018). Another benefit is that each phase of the

* Corresponding author at: Department of Electrical Engineering, Graphic Era (Deemed to be University), Dehradun 248002, India.
E-mail addresses: jabari97@sut.ac.ir (M. Jabari), sekinci@beu.edu.tr (S. Ekinci), davutizci@uludag.edu.tr, davutizci@gmail.com (D. Izci), mohitbajaj.ee@geu.ac.in (M. Bajaj), vojtech.blazek@vsb.cz (V. Blazek), lukas.prokop@vsb.cz (L. Prokop).

https://doi.org/10.1016/j.egyr.2026.109231
Received 29 November 2025; Received in revised form 12 February 2026; Accepted 8 March 2026
Available online 13 March 2026
2352-4847/© 2026 The Authors. Published by Elsevier Ltd. This is an open access article under the CC BY license (http://creativecommons.org/licenses/by/4.0/).

Nomenclature

SRM	Switched reluctance motor
IM	Induction motor
AI	Artificial intelligence
FC	Fuzzy control
HC	Hysteresis control
HIL	Hardware in the loop
ITAE	Integral of time-weighted absolute error
ITSE	Integral of time-weighted square error
MPC	Model predictive control
SMC	Sliding mode control
HOA	Hybrid observer algorithm
SRG	Switched reluctance generator
MPPT	Maximum power point tracking
PI	Proportional integral
GWO	Gray wolf optimization
PID	Proportional integral derivative
PID*n*	Proportional integral derivative with derivative filter
MWOA	Modified whale optimization algorithm
FOPI	Fractional order proportional integral
PWM	Pulse-width modulation
WOA	Whale optimization algorithm
ANFIS	Adaptive neuro-fuzzy inference system
$\mathbf{V}_{in}$	Input voltage
$\mathbf{R}_s$	Resistance of per-phase stator
ω_m	Motor's angular velocity
$\mathbf{T}_L$	Load torque
$\mathbf{T}_{ripple}$	Torque ripple value
$\mathbf{T}_{min}$	Minimum torque value
$\Delta\mathbf{C}$	Current error
$\mathbf{t}_{sim}$	Simulation time
$\mathbf{C}_1$, $\mathbf{C}_2$	Acceleration coefficients
$\mathbf{K}_{P\text{-}C}$, $\mathbf{K}_{P\text{-}S}$, $\mathbf{K}_{PP\text{-}S}$, $\mathbf{K}_{PP\text{-}C}$	Proportional gains of cascaded controller
$\mathbf{K}_{D\text{-}C}$, $\mathbf{K}_{D\text{-}S}$	Derivative gains of cascaded controller
$\mathbf{U}_{B\text{-}H}$	Upper hysteresis band
r.p.m	Revolutions per minute
I_{ref}	Reference current
I_{ph}	Per-phase current
$\mathbf{T}_r$	Rise time
$\mathbf{T}_s$	Settling time
$\mathbf{T}_p$	Peak time
ΔI_1	Multi stage controller's initial stage control signal
PMM	Permanent magnet motor
FOPID	Fractional order proportional integral derivative
ITC	Indirect torque control
ILC	Iterative learning control
AMPC	Adaptive model predictive control
IAE	Integral of absolute error
ISE	Integral of square error
x	Simulation time in second
DCC	Dead beat current control
NN	Neural network
SVPDPI	Switching variable proportional desaturation proportional integral
DTC	Direct torque control
LUS	Local unimodal sampling
ACO	Ant colony optimization
SHO	Spotted hyena optimization
PSO	Particle swarm optimization
FOPI(1+PID*n*)	Fractional order proportional integral one plus proportional integral derivative with derivative filter
PSO-TVAC	Particle swarm optimization with time-varying acceleration coefficients
TSA	Tree seed algorithm
DEO	Differential evolution optimization
FPO	Flower pollination optimization
CF	Cost function
$\mathbf{i}_s$	Current in the stator winding
θ	Rotor position
J	Moment of inertia
F_ω	Coefficient of friction
$\mathbf{T}_{max}$	Maximum torque value
$\mathbf{T}_{avg}$	Mean torque value
$\Delta\mathbf{S}$	Speed error
$\mathbf{C}_{1f}$, $\mathbf{C}_{2f}$	Social acceleration factors
$\mathbf{C}_{1i}$, $\mathbf{C}_{2i}$	Initial and final values of cognitive
e(t)	Error signal between speed and current
$\mathbf{K}_{I\text{-}C}$, $\mathbf{K}_{I\text{-}S}$, $\mathbf{K}_{II\text{-}S}$, $\mathbf{K}_{\text{II-C}}$	Integral gains of cascaded controller
$\boldsymbol{\lambda}$, $\boldsymbol{\mu}$	Integral and derivative order
$\mathbf{L}_{B\text{-}H}$	Lower hysteresis band
θ_{on}, θ_{off}	Turn on and turn off angles
ω_{ref}	Reference value for angular velocity
$\mathbf{T}_e$	Motor electric torque
OS	Overshoot
$\Delta\omega$	Speed deviation
ΔI	Controller output signal

SRM is electrically separate, which increases safety and fault tolerance (Al-Amyal et al., 2023).

Despite the above advantages, however, keeping SRMs stable and efficient under different working conditions is not easy. These motors are nonlinear, and their performance can be affected by load changes, parameter errors, and power fluctuations (Wei et al., 2021; Wang et al., 2012). Such issues can lead to higher torque ripple, poor speed control, and lower efficiency. Therefore, choosing the right controller is very important to ensure smooth and reliable operation.

The double-salient structure of SRMs causes large torque ripple, which creates vibration, noise, and energy loss. At the same time, accurate speed control is needed for many applications (Pan et al., 2017; Sun et al., 2023; Uddin et al., 2016). Many researchers have studied different control methods to solve these problems. These include classic proportional-integral-derivative (PID) and fractional-order PID (FOPID) controllers (Kumar and Chidanandappa, 2024; Jabari et al., 2025a), Kalman filters (Elsisi et al., 2023), look-up-table models (Memon et al., 2020), and optimization-based tuning (Jabari and Rad, 2024). In most cases, a closed-loop control system is used with both speed and current controllers. The actual torque is estimated from the rotor position and current, and the switches are adjusted based on this feedback (Fang et al., 2021; Sun et al., 2019). These methods focus on reducing torque ripple and improving speed tracking (Senthil Murugan and Maruthupandi, 2020). Common speed controllers include fuzzy control (FC) (Song et al., 2021; Elsisi et al., 2024), PID (Jabari et al., 2025a), and iterative learning control (ILC) (Mahalakshmi and Kanthalakshmi, 2022). For current control, techniques such as current chopping (Memon et al., 2023; Peng et al., 2015) and intelligent ILC-based control (El-Kharahi et al., 2015) are often used. Some studies have also proposed linear models to make the SRM easier to control (Ahmad and Narayanan, 2016; Huang et al., 2016).

In recent years, optimization and artificial intelligence (AI) have been used to make control systems more robust and efficient. Adaptive model predictive control (AMPC) (Elsisi, 2024) and other AI-based strategies have shown good results under uncertain and changing conditions (Mohamed et al., 2022). Similar methods have also been applied

Table 1
An overview of the control techniques and optimization algorithms employed in recent years.

Article	Proposed algorithm	Solving method	Objective function	Contribution
Oshaba, et al. (Oshaba et al., 2015)	ACO	PI controller	Integral of time multiply absolute error	Enhance the efficiency of the speed regulator for the SRM
Sun, et al. (Sun et al., 2019)	N.O	Fast modeling method for a segmented-rotor and PI controller	N.O	The suggested method has effectively reduced torque and achieved consistent speed stability
Martin and Kumar (Martin and Kumar, 2021)	MCSPSO	PI controller	Integral time squared error	Obtain better torquereduction and speed control
Song, et al. (Song et al., 2021)	N.O	Improved fuzzy and PID controller	N.O	Improves the response speed of the system and decreases torque ripple
Kotb, et al. (Kotb et al., 2022)	LUS and SHO	PID controller	Integral sum of squared error multi-objective function	The motor's speed is efficiently managed, and there is a partial reduction in torque ripples
Al-Amyal, et al. (Al-Amyal et al., 2023)	ACO	PID controller	Integral sum of squared error multi-objective function	Minimizing torque ripples, enhancing motor efficiency, and avoiding the generation of significant reverse torque
Jabari and Rad (Jabari and Rad, 2024)	Two metaheuristic algorithms: Dung Beetle Optimizer (DBO) and Ant-Lion Optimizer (ALO)	Cascaded PID and FOPID controllers	cumulative sum of squared errors in speed and current over time	Enhanced speed tracking, reduced torque ripple, and improved current profile using DBO and ALO-based optimization under static and dynamic loads.
Gengaraj, et al. (Gengaraj et al., 2023)	DEO and FPO	TSF and PID controller	Integralsquare error	The proposed approach has successfully decreased torque ripples in SRM when compared to the Differential Evolution (DE) algorithm
Jabari, et al. (Jabari et al., 2025a)	HALO	Cascaded PID and FOPID controllers	cumulative sum of squared errors in speed and current over time	Reduces torque ripple, enhances response speed, and improves tracking accuracy in a short time

N.O: Not mentioned

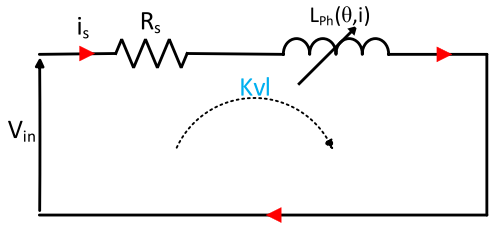


Fig. 1. Equivalent circuit in SRM for one-phase.

in other complex systems, such as autonomous vehicles, microgrids, and energy storage systems (Elsisi, 2024; Elsisi et al., 2021; Bergies et al., 2022; Agajie et al., 2023). Other advanced control methods include model predictive control (MPC), dead-beat current control (DCC) (Zhang et al., 2019; Hu et al., 2020), and sliding mode control (SMC) (Hu et al., 2019; Divandari et al., 2019). Recent studies demonstrate that intelligent, bio-inspired, and hybrid optimization techniques have significantly advanced nonlinear control performance. Metaheuristic algorithms have been effectively applied to DC motor and liquid-level systems (Ekinci et al., 2025), neural and sliding-mode synchronization in chaotic and multi-agent environments (Turab et al., 2025; Al Samman et al., 2025), and renewable-energy applications through optimized PID and cascaded control structures (Gupta et al., 2025; Izci et al., 2025; Jabari et al., 2025b; Hussein et al., 2025). Further developments in automatic voltage regulation and dynamic stability using refined sinh–cosh, mountain gazelle, and gradient-based optimizers (Jan et al., 2025; Izci et al., 2024a, 2024b; Aribowo et al., 2024), along with high-precision aerospace pitch control via sinh–cosh and artificial-rabbits-based designs (Abualigah et al., 2024a, 2024b), consistently highlight the capability of adaptive and nature-inspired controllers to achieve rapid response, improved damping, and high steady-state accuracy across complex nonlinear systems. Advanced strategies such as sliding-mode control (SMC), including finite-/-fixed-time and gain-adaptive variants, have demonstrated strong disturbance rejection in multi-level converter and drive applications, though they typically require careful chattering suppression, observer design, and may increase switching activity. Recent examples include gain-adaptive or varying-exponent SMC on NPC converters and finite-time SMC with enhanced disturbance compensation (Shen et al., 2024). Model predictive control (MPC) from finite-set MPC to predictive current/torque control achieves fast dynamics and ripple reduction but incurs non-trivial on-line computation and accurate model requirements at the converter-sampling rate. Recent SRM/converter studies illustrate these trade-offs (Mohanraj et al., 2024). Dead-beat current control (DCC) offers one-step tracking but is sensitive to parameter/time-delay mismatch and quantization unless augmented with observers and delay compensation, as reflected in recent designs for SRM/PM machines (Liu et al., 2024).

Several recent studies have tested new hybrid controllers. Shadhik and Senthil Kumaran (Shadhik and Senthil Kumaran, 2023) improved the performance of a switched reluctance generator (SRG) using grey wolf optimization (GWO) with a PI controller. Oubouaddi et al. (Oubouaddi et al., 2022) compared PID, neural-network, and fuzzy controllers, showing that combining AI with classic control improves speed regulation. Saha and Mishra (Saha and Mishra, 2023) developed a modified whale optimization algorithm with a fractional-order PI (MWOA-FOPI) controller that reduced torque ripple and improved speed tracking. Martin and Kumar (Martin and Kumar, 2021) used a PWM-PI controller with bio-inspired optimization to enhance speed control. Senthil Murugan and Maruthupandi (Senthil Murugan and Maruthupandi, 2020) created a hybrid observer algorithm (HOA) combining ANFIS and fuzzy-PID to estimate rotor position and speed without extra sensors. Other optimization methods, such as ant colony optimization (ACO) (Oshaba et al., 2015), spotted hyena optimizer (SHO), and local unimodal sampling (LUS) (Kotb et al., 2022), have also shown improvements. Particle swarm optimization (PSO) has been used for PID tuning (Nimisha and Senthilkumar, 2018), and improved direct torque control (DTC) methods have been reported (Yang et al., 2022). Gengaraj et al. (Gengaraj et al., 2023) suggested using a torque-sharing function (TSF) with flower pollination optimization (FPO) to further reduce ripple.

Although many control methods have been studied, it is still difficult to achieve stable and efficient performance for SRMs in all conditions. Nonlinearity remains a major challenge, and some controllers are complex or not robust enough. Therefore, this study proposes a simple but effective controller to improve speed tracking and reduce torque ripple while keeping the system practical and reliable. The main findings

Table 2
Parameters of the analyzed 6/4 SRM.

SRM parameters	Rated voltage	Rated power	Rated speed	Turn off angle	Turn on angle	Stator resistance	Inertia	Friction
Values	240 V_{dc}	60 kW	3000 rpm	75°	45°	0.05 Ω	0.05 kg.m^2	0.02 N.m.s

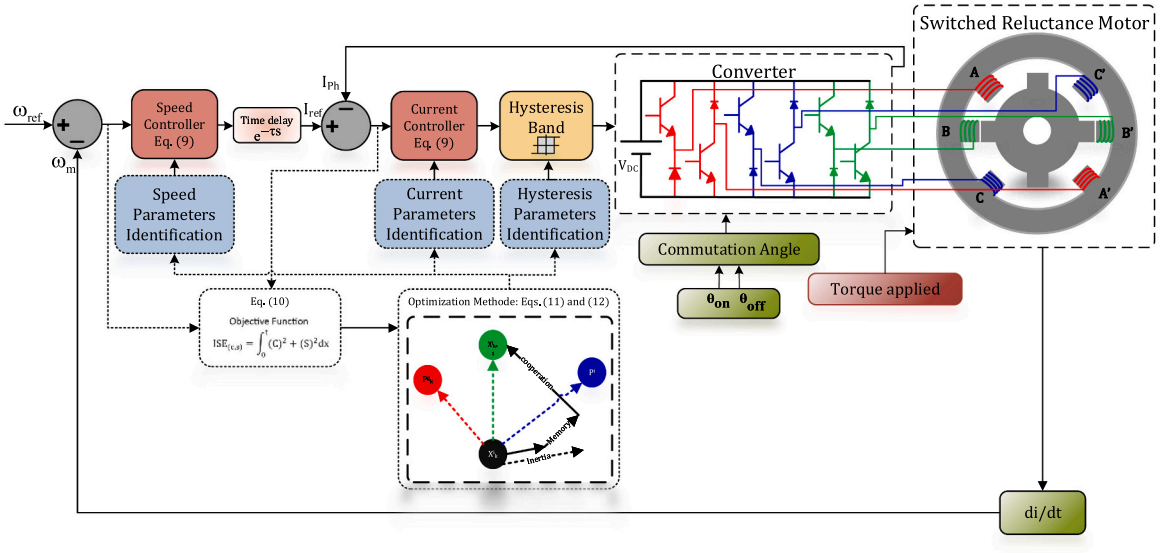


Fig. 2. General scheme of the under-examination model.

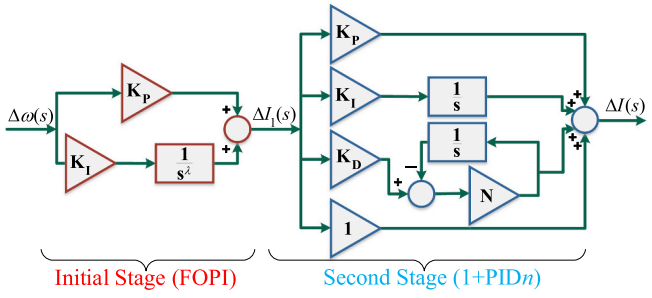


Fig. 3. Proposed FOPI(1 +PID*n*) controller structure.

from these recent studies are summarized in Table 1.

Previous research on SRM control can be broadly classified into four categories.

(1) Classical linear controllers, such as PI, PID, and fractional-order PID (FOPID), are simple and efficient but often fail to preserve performance under strong nonlinearities and parameter variations.
(2) Intelligent and learning-based controllers, including fuzzy logic and iterative learning control (ILC), improve adaptability but demand extensive tuning and may suffer from slow convergence.
(3) Current and torque control techniques, such as hysteresis PWM, direct torque control (DTC), and torque sharing functions (TSF), are effective for torque ripple reduction but do not adequately address speed-loop disturbances.
(4) Advanced robust and predictive strategies, such as model predictive control (MPC), dead-beat current control (DCC), and sliding mode control (SMC), provide excellent dynamic response but require high computational resources and accurate models, which limit their real-time deployment in cost-sensitive SRM drives.

Despite notable progress in SRM control research, several important challenges remain unresolved. One key issue is the limited understanding and treatment of nonlinear effects in SRM operation. Many existing control strategies struggle to maintain high efficiency and stability when the motor operates under variable and demanding conditions. Nonlinear factors such as magnetic saturation and time delays act as strong disturbances that can decrease motor performance and increase energy losses, especially when traditional controllers are used (Dang et al., 2020; Hameed et al., 2023).

Time delays, in particular, play an important role as nonlinear disturbances in SRM systems. Considering these effects in controller design can help predict system behavior more accurately and improve performance. Therefore, developing control strategies that can effectively handle such nonlinearities is essential. The integration of classical control approaches with advanced optimization methods represents a promising yet underexplored direction for improving system performance.

In this study, a fractional-order proportional–integral controller with an additional derivative filter, called FOPI (1+PID*n*), is proposed to address these issues. This controller aims to combine the simplicity and robustness of classical control with the flexibility and precision of modern fractional-order and optimization-based techniques. Such a design is particularly suitable for SRMs, where achieving stable and robust performance under a wide range of conditions is still a major challenge.

The performance of the proposed approach is assessed by comparing it with both conventional controllers, such as the PID, and advanced ones, including the FOPI optimized via the PSO-TVAC algorithm. This analysis demonstrates that the proposed FOPI(1 +PID*n*) controller not only addresses the existing research gaps but also provides improved dynamic response, better stability, and higher overall performance across different motor operating conditions (Jabari and Rad, 2024). To address the challenges of torque ripple reduction and speed control in SRMs this study introduces a novel approach through the design of a multi-stage controller. The key contributions of this work are summarized as follows:

Table 3
Range of gains in proposed and other controllers.

Gains	$K_{P\text{-}S}$	$K_{I\text{-}S}$	$K_{D\text{-}S}$	$K_{P\text{-}C}$	$K_{I\text{-}C}$	$K_{D\text{-}C}$	λ	μ	$U_{B\text{-}H}$	$L_{B\text{-}H}$	N
Lower limit(min)	0	0	0	0	0	0	0.01	0.01	0	-20	0.01
Upper limit(max)	20	20	20	20	20	20	2	2	20	0	1000

Table 4
Values of the CF following five rounds of optimization algorithms using various controllers.

Algorithm	PSO-TVAC				TSA				GWO			
Controller	Proposed	FOPID	PID*n*	PID	Proposed	FOPID	PID*n*	PID	Proposed	FOPID	PID*n*	PID
Best	0.9052	1.3223	0.985	1.3952	1.0008	1.2308	1.1254	1.6701	1.126	1.4101	1.4985	1.7801
Worst	1.3506	1.6215	1.4678	1.6854	1.5089	1.7089	1.7566	2.2032	1.2503	1.9013	2.1456	2.1202
Mean	0.7314	1.2625	0.8022	1.5217	1.3432	1.4543	1.5132	1.8001	1.1444	1.1821	1.5335	1.8301

1. This paper introduces the FOPI (1 +PID*n*) controller, a multi-stage controller that integrates the advantages of fractional order controllers with traditional PID controllers enhanced by a derivative filter (PID*n*). This controller is uniquely tailored for super-fast speed tracking and effective torque ripple minimization in SRMs, offering a simpler yet more efficient solution compared to existing control strategies.
2. The proposed controller is rigorously evaluated across a range of challenging operating conditions, including sudden load changes, time delays as nonlinear factors, and parameter uncertainties. The FOPI (1 +PID*n*) controller consistently demonstrates superior dynamic response and stability, ensuring reliable motor performance even in adverse scenarios.
3. A comprehensive comparison is conducted between the FOPI (1 +PID*n*) controller and other advanced controllers, such as PID, PID*n*, and FOPID controllers optimized using the PSO-TVAC algorithm. The results underscore the enhanced performance of the proposed controller, particularly in terms of speed regulation and torque ripple reduction, establishing its potential as a superior control strategy for SRMs.

These contributions not only introduce an effective solution to existing challenges in SRM control but also provide a significant advancement in the development of robust, high-performance controllers for electric motors.

This paper is structured into six distinct sections: Section 1 provides an introduction, while Section 2 introduces and elucidates the details of the SRM and in the Section 3, the introduction and analysis of the proposed FOPI(1+PID*n*) controller is discussed. Section 4 outlines the problem formulation and briefly summarizes the integration of the PSO-TVAC optimization technique with the proposed controller. Section 5 presents the results of control strategy evaluations, various scenarios, and comparative analyses. Finally, Section 6 serves as the conclusions and future works of the paper.

2. Mathematical model of the switched reluctance motor

A mathematical model for comprehending the operation of an SRM can be developed through an analysis of its electrical schematic, considering two critical parameters: phase resistance and phase inductance. The single-phase schematic, shown in Fig. 1, provides an overview of the electrical paths within the motor. According to the mathematical representation of the 6/4 SRM, the circuit can be specified as follows (Yang et al., 2022):

$$V_{in} = R_s i_s + \frac{d\lambda(i,\theta)}{dt} \tag{1}$$

where V_{in}, i_s, R_s, and $\lambda\ (i, \theta)$ shown the input voltage applied to per-phase of the SRM, current in the stator winding, resistance of per-phase stator, and flux linkage, respectively. θ is the rotor position. The per-phase flux linkage $\lambda\ (i, \theta)$ is given by:

$$\lambda(i,\theta) = i\,L(i,\theta) \tag{2}$$

On the other side, $T_e(i, \Theta)$ represents the electromagnetic torque, which is obtained from the SRMs coenergy (Kotb et al., 2022).

$$T_e(i,\theta) = \frac{\partial \acute{\omega}\ (i,\theta)}{\partial\theta} \tag{3}$$

The expression $\acute{\omega}\ (i,\theta)$ refers to coenergy and is derived follows:

$$\acute{\omega}\ (i,\theta) = \int_0^i \lambda(i,\theta) \tag{4}$$

The total electromagnetic torque T_e is the combined torque from all phases produced by the SRM.

$$T_e = J\frac{d\omega}{dt} + F_\omega \omega_m + T_L \tag{5}$$

where ω_m refers to the motor's angular velocity, J represents the moment of inertia, T_L signifies the load torque, and F_ω denotes the coefficient of friction. Finally, the torque ripple of the SRM is obtained from the following equation:

$$T_{ripple} = \frac{T_{\max} - T_{\min}}{T_{avg}} \tag{6}$$

Here, $T_{\min}$ represents the minimum torque value, $T_{\max}$ represents the maximum torque value, and T_{avg} signifies the mean torque value. This work has been done in MATLAB/Simulink environment to model SRM 6/4 using mathematical modeling. The parameters used in SRM modeling in this research work are listed in Table 2. Also, an overview of the studied SRM and controllers is shown in Fig. 2.

3. Proposed FOPI(1+PID*n*) controller

The controller under discussion leverages a combination of the FOPI and the PID*n* controllers. This approach distinguishes it from traditional FOPI and PID controllers, as it combines the advantages of both types. This distinctive combination leads to improved control performance, effectively capturing the dynamics of the process for precise control. The suggested multi-stage controller is more stable and robust to clearing errors and disturbances. Reducing settling time, overshooting, and oscillations promotes a quick and smooth system response. The FOPI controller includes fractional order operators in addition to common and pure proportional and integral operators, giving it more design freedom (Jabari et al., 2025a; Shayeghi et al., 2023). System stability, responsiveness, and steady-state error are improved by this combination. Furthermore, the PID*n* controller includes a derivative N-filter to fine-tune responses to fluctuations in the error signal while better simulating real-world derivative control action functions. The schematic of the proposed controller is shown in Fig. 3.

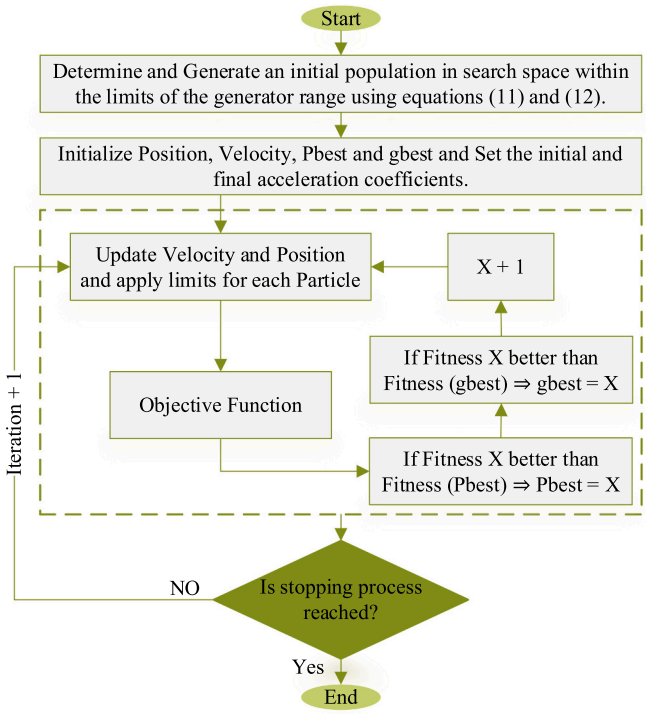


Fig. 4. Flow chart for selecting the optimal parameters by PSO-TVAC.

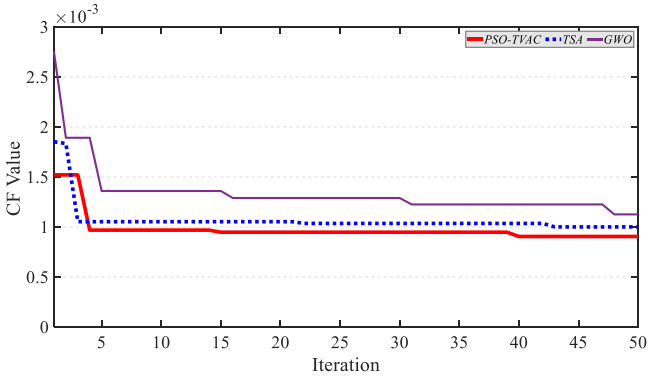


Fig. 5. The best results of the CF by running the PSO-TVAC, TSA and GWO algorithms with the proposed controller.

$$G_{FOPI}(s) = \frac{\Delta I_1(s)}{\Delta \omega(s)} = K_P + \frac{K_I}{s^{\lambda}} \tag{7}$$

$$G_{PIDn}(s) = \frac{\Delta I(s)}{\Delta I_1(s)} = K_P + \frac{K_I}{s} + \frac{sK_DN}{s+N} \tag{8}$$

$$G_{FOPI(1+PIDn)}(s) = \frac{\Delta I(s)}{\Delta \omega(s)} = \left(K_P + \frac{K_I}{s^{\lambda}}\right)\left(1 + K_P + \frac{K_I}{s} + \frac{sK_DN}{s+N}\right) \tag{9}$$

Hence, the suggested controller exhibits these three primary attributes:

- Enhanced system response: The FOPI component introduces fractional order operators that quicken the system's response to changes and disturbances.
- Reduced steady-state error: By utilizing fractional order operators, the FOPI(1 +PID*n*) controller diminishes the steady-state error, ensuring that the system maintains accuracy even over extended periods.

Table 5
Optimum gains of proposed and other controllers.

Controller Values			
FOPI(1+PID*n*)	FOPID	PID*n*	PID
$K_{P-S} = 0.014$, $K_{I-S} = 1.419$, $K_{D-S} = 0.043$, $K_{P-C} = 20$, $K_{I-C} = 7.010$, $K_{D-C} = 0$, $K_{PP-S} = 3.510$, $K_{II-S} = 4.030$, $K_{PP-C} = 20$, $K_{II-C} = 12.880$, $U_{B-H} = 1.979$, $L_{B-H} = -3.405$, $\lambda_S = 0.010$, $\lambda_C = 0.04$, $N_S = 183.611$, $N_C = 747.520$	$K_{P-S} =$ 1.8632, $K_{I-S} =$ 6.521, $K_{D-S} =$ 0.385, $K_{P-C} =$ 5.576, $K_{I-C} =$ 14.869, $K_{D-C} =$ 0, $U_{B-H} =$ 10.244, $L_{B-H} =$ − 3.092, $\lambda_S =$ 1.643, $\lambda_C =$ 0.13, $\mu_S =$ 0.545, $\mu_C =$ 0.167	$K_{P-S} =$ 15.265, $K_{I-S} =$ 19.093, $K_{D-S} =$ 0.828, $K_{P-C} =$ 17.783, $K_{I-C} =$ 1.844, $K_{D-C} =$ 13.622, $U_{B-H} =$ 20, $L_{B-H} =$ − 15.306, $N_S =$ 186.295, $N_C =$ 0.010	$K_{P-S} =$ 2.982, $K_{I-S} =$ 1.191, $K_{D-S} =$ 0, $K_{P-C} =$ 0.760, $K_{I-C} =$ 20, $K_{D-C} =$ 0, $U_{B-H} =$ 7.337, $L_{B-H} =$ 0

- Improved stability and fine-tuned control: The PID*n* component provides fine-tuned control with the ability to customize the derivative filter, enhancing system stability and adaptability to unique system characteristics.

From a theoretical perspective, the improved performance of the proposed FOPI(1+PID*n*) controller arises from its hybrid fractional and integer-order dynamics. The fractional-order stage introduces non-local memory and adjustable phase characteristics, allowing smoother phase-lead and phase-lag behavior and improved robustness to parameter variations. Meanwhile, the derivative-filtered PID*n* stage ensures rapid transient response while effectively suppressing high-frequency noise. The cascade configuration therefore combines low-frequency accuracy with high-frequency adaptability, achieving enhanced gain and phase margins, reduced overshoot, and faster convergence to the reference speed under nonlinear and uncertain operating conditions.

4. Optimization strategy

Choosing an optimization approach for the control system is of considerable importance. In practical applications, optimized controllers show better and more robust performance. Controller performance, without optimization, is likely to be unsatisfactory. Even the most accurate controllers in the industry may perform poorly if not configured with appropriate parameters, leading to suboptimal performance of the designed system. This defect in the design of the motor controller can appear in the form of energy loss and reduced motor efficiency. Therefore, in this section, we define the appropriate cost function. We define this function to optimize controller parameters and optimize motor output in different operating mode. After that, we discuss the solution strategy of this optimization.

4.1. Cost function definition

The cost function (CF) shows the designer's prediction of the dynamic response of the system. It is expected that the output of the desired control mechanism can give us the best solution under different operating mode, which includes eliminating the steady-state error of the system. The nonlinear effects such as time delay and short-term load or torque disturbances can create a complex operating mode for the SRM. However, the ultimate goal of this statement is to maintain the balance between the output speed and the motor torque. The cost function used must be robust to variations in operating mode, aiming to achieve the

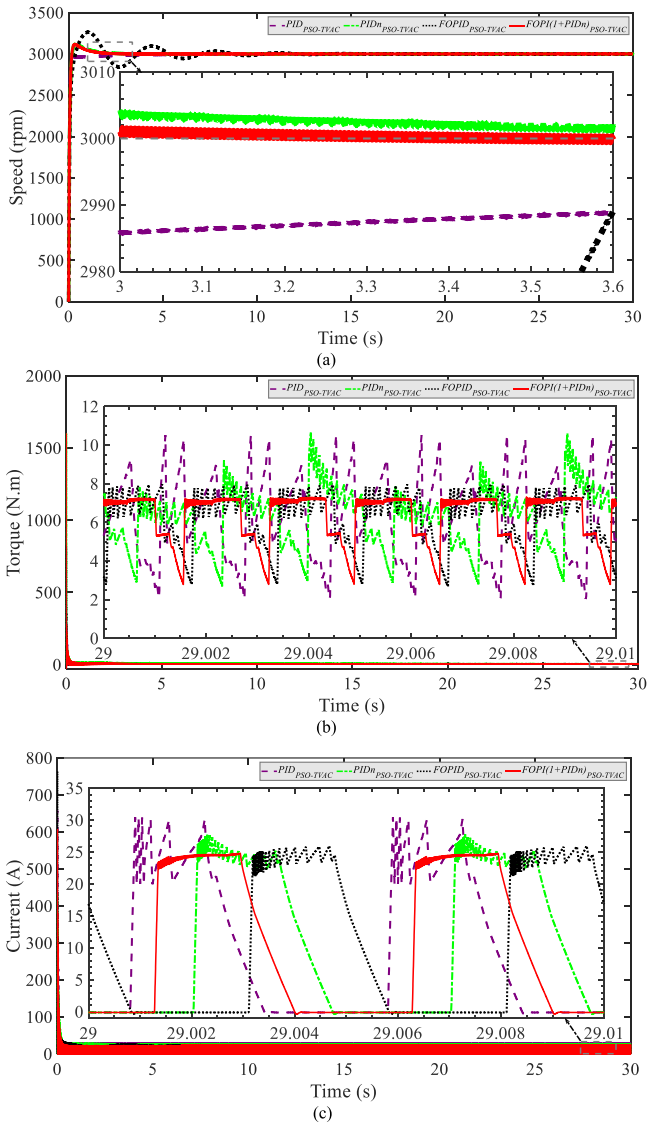


Fig. 6. Time response of (a) Speed, (b) Total torque, (c) Phase current for proposed and other controllers in Case 1.

Table 6
Transient response specifications in case 1.

Controller	T_r	T_s	T_p	OS
PID	0.08735	0.1486	26.487	0.0040
PID*n*	0.10736	0.9594	0.3713	4.0245
FOPID	0.15021	4.8976	1.0414	8.7865
FOPI(1 +PID*n*)	0.09618	0.8248	0.334	3.8859

system's optimal dynamic response when exposed to disturbance signals and short-term load applications. The cost function applied in this manuscript is as follows.

$$CF_{\min} = \int_0^{t_{sim}} \left[(\Delta S)^2 + (\Delta C)^2\right] dt \tag{10}$$

Here, ΔS, ΔC and t_{sim} are speed error, current error and simulation time, respectively. It should be noted that although torque ripple is not explicitly included as a separate objective term, torque in SRM systems is strongly coupled with phase current dynamics. Therefore, minimizing current tracking error indirectly contributes to ripple reduction. Extension of the cost function toward a multi-objective formulation including torque ripple or switching-loss penalties can be considered in future work.

Table 7
Comparison of the torque values and torque ripples in case1.

Controller	T_{max}	T_{min}	T_{avg}	$\%T_{ripple}$
PID	10.53	2.04	6.29	134.88
PID*n*	10.68	2.69	6.28	127.14
FOPID	7.98	2.66	6.28	84.70
FOPI(1 +PID*n*)	7.32	2.79	6.28	72.04

The CF is restricted by the range of controller coefficients, defining the search space for the optimization problem as presented in Table 3.

4.2. Optimization method

In the new type of PSO, denoted as PSO-TVAC. the acceleration coefficients are dynamically and linearly changed during the iteration, deviating from the conventional use of static coefficients. The research shows that PSO-TVAC skillfully explores the search space in the early stages and has a faster convergence to the global optimum in the later stages. This adaptive approach increases the optimal performance of the algorithm and shows promising results for optimization tasks (Rahnama, n.d.). The representation of acceleration coefficients C_1 and C_2 is given by:

$$C_1 = \left(C_{1f} - C_{1i}\right)\frac{iter}{iter_{\max}} + C_{1i} \tag{11}$$

$$C_2 = \left(C_{2f} - C_{2i}\right)\frac{iter}{iter_{\max}} + C_{2i} \tag{12}$$

where C_{1f}, C_{2f}, C_{1i} and C_{2i} are social acceleration factors and initial and final values of cognitive respectively. Also, $C_{1f} < C_{1i}$ and $C_{2f} < C_{2i}$. This algorithm can be divided into the following key steps:

- Initialization: A population of particles is initialized within the solution space, each possessing random positions and velocities.
- Fitness evaluation: The fitness of each particle is assessed based on its current position.
- Personal and global best: Each particle updates its personal best position, reflecting its individual experience, and the global best position, representing the collective experience within its neighborhood.
- Update particle velocities and positions: The velocity and position of the particles are readjusted using time-varying acceleration coefficients.
- Update acceleration coefficients: Time-varying acceleration coefficients are adjusted according to a predefined strategy or function.
- Repeat and stopping process: The algorithm iteratively performs steps 2–5 until termination conditions are met, which commonly involve reaching a specified tolerance limit or completing a predetermined maximum number of iterations in stochastic optimization algorithms.

The convergence behavior of PSO-TVAC was verified through repeated independent runs. Increasing the number of iterations beyond 50 resulted in marginal improvement in CF values (<1%), confirming that 50 iterations are sufficient for stable convergence. The limited dispersion between best, worst, and mean values reported in Table 4 further demonstrates repeatability and robustness against stochastic initialization.

The step-by-step process of implementing the algorithm is illustrated in Fig. 4.

Table 8
Time-based indicators illustrating the dynamic response of the SRM in case 1.

Controller	ISE × 10^4		IAE × 10^4		ITSE × 10^4		ITAE × 10^4	
	Speed	Current	Speed	Current	Speed	Current	Speed	Current
PID	1.418	0.7833	61.66	224.2	0.05287	6.894	81.89	3240
PID*n*	1.18	0.6377	62.87	202.3	0.06336	7.079	43.81	3073
FOPID	2.044	0.6686	224.2	203	1.275	7.144	650.1	3021
FOPI(1 +PID*n*)	1.098	0.6265	55.48	243	0.04829	8.606	37.02	3841

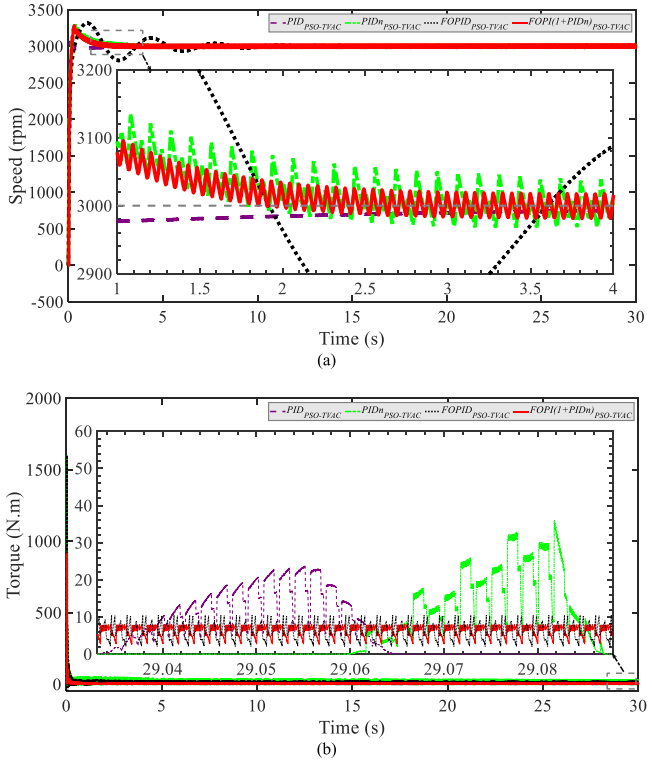


Fig. 7. Time response of (a) Speed, (b) Total torque, with time-delay for proposed and other controllers in Case 1.

Table 9
Transient response specifications with delay time in case 1.

Controller	T_r	T_s	T_p	OS
PID	0.072103	0.16269	0.1493	2.3862
PID*n*	0.10606	2.0652	0.34988	9.7502
FOPID	0.13391	6.2979	1.0034	10.6209
FOPI(1 +PID*n*)	0.10566	1.5431	0.30652	9.7905

Table 10
Comparison of the torque values and torque ripples in case 1.

Controller	T_{max}	T_{min}	T_{avg}	$\%T_{ripple}$
PID	23.78	0.00	6.40	371.44
PID*n*	36.10	–0.02	6.68	540.78
FOPID	10.53	1.96	6.28	136.39
FOPI(1 +PID*n*)	7.99	2.67	6.28	84.68

5. Simulation and discussion

In this section, we put the proposed FOPI (1 +PID*n*) controller into action, enabling it to perform the control function within the SRM as previously discussed in Section 3. A survey of the literature with the laboratory experiments shows that the results of the MATLAB-based

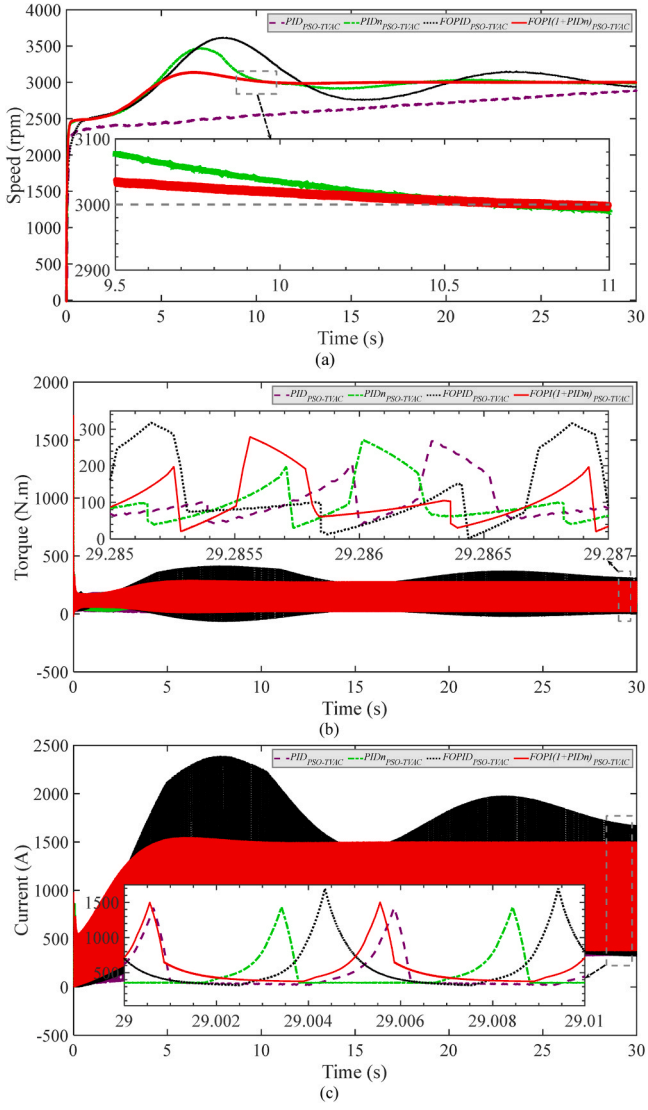


Fig. 8. Time response of (a) Speed, (b) Total torque, (c) Phase current for proposed and other controllers in Case 2.

simulations are very close to their performance in the real-world studies, and that these results in classical controllers cover each other well (Xiu et al., 2023; Scalcon et al., 2022; Ren et al., 2022). So, the closed-loop system is implemented in the MATLAB 2023a using Simulink. It is worth clarifying that the PSO-TVAC optimization is performed offline, prior to the control tests, to obtain a fixed set of controller parameters. Therefore, the optimization routine is not executed inside the real-time control loop. During online operation, the controller only evaluates the cascaded FOPI and PIDn laws. Hence, the additional computational burden in real-time is limited to standard controller and filter evaluations and does not include iterative metaheuristic optimization. Through 50 iterations and the involvement of 20 particles, the

Table 11
Transient response specifications in case 2.

Controller	T_r	T_s	T_p	OS
PID	12.2398	26.3859	29.9987	0.1750
PID*n*	3.4737	16.0771	7.0581	16.0173
FOPID	3.1536	28.0233	8.3045	23.0481
FOPI(1 +PID*n*)	3.3007	8.9901	6.6154	4.7514

Table 12
Comparison of the torque values and torque ripples in case 2.

Controller	T_{max}	T_{min}	T_{avg}	$\%T_{ripple}$
PID	267.41	38.64	103.83	220.34
PID*n*	270.27	30.42	99.56	240.92
FOPID	317.63	1.47	131.01	241.12
FOPI(1 +PID*n*)	278.86	20.10	107.82	239.99

PSO-TVAC algorithm has identified the optimal controller coefficient values. The simulation duration is set at 30 s. The fractional-order operators $(s^{\lambda}, and s^{\mu})$ in the proposed FOPI(1+PID*n*) controller were implemented using the FOMCON toolbox in MATLAB/Simulink (Tepljakov and Tepljakov, 2017; Shayeghi and Rahnama, 2022). The operators are approximated through the Oustaloup recursive filter method, which provides an accurate frequency-domain realization of fractional integrators and differentiators. The approximation was configured over a frequency range of [0.001, 1000] rad/s with an approximation order of five, which yielded stable and accurate results without significant deviation for higher orders. Design parameter specifications used in this study are shown in appendix.

Adequate iterations of the PSO-TVAC algorithm have been carried out, ensuring the algorithm's convergence to the optimal point. To assess the efficiency of the proposed controller, we employ the PSO-TVAC technique for optimization. Fig. 5 provides a visual representation of the results obtained from this optimized implementation, demonstrating the achievement of the lowest CF values after 50 iterations. This effectively underscores the controller's superior performance. The PSO-TVAC optimization algorithm has been separately run on five rounds, and Table 4 displays the best, worst, and the average of the CF values obtained with various controllers. Eventually, Table 5 provides the optimal controller parameter values obtained from the best results achieved by the PSO-TVAC algorithm.

For a more comprehensive numerical comparison, the calculation and reporting of time domain evaluation indices, namely integral of square error (ISE), integral of time-weighted square error (ITSE), integral of absolute error (IAE), and integral of time-weighted absolute error (ITAE), have been performed in each scenario. It is worth noting that the proposed control architecture does not require real-time iterative optimization. The online computational effort is limited to evaluating cascaded controller equations and low-order filtering operations. Therefore, the execution complexity scales linearly with sampling frequency and is suitable for digital signal processor (DSP) or microcontroller implementation in industrial SRM drives.

The equations pertaining to these indicators are provided in (13)-(16) where, x is simulation time in s, and e(t) is an error signal between speed and current in SRM.

$$ISE = \int_0^x e^2(t)dt \tag{13}$$

$$ITSE = \int_0^x t.e^2(t)dt \tag{14}$$

$$IAE = \int_0^x |e(t)|dt \tag{15}$$

$$ITAE = \int_0^x t.|e(t)|dt \tag{16}$$

5.1. Case 1: no load

In this case, the motor is operating without any external load. We assess the output speed, torque, and motor current by setting the reference speed to 3000 rpm. The speed response is shown in the Fig. 6 (a) by applying no-load operation to the SRM. As it is known, FOPI (1+PID*n*), PID*n*, PID, FOPID controllers show the best response in

Table 13
Time-based indicators illustrating the dynamic response of the SRM in case 2.

Controller	ISE $\times 10^{-4}$		IAE $\times 10^{-4}$		ITSE $\times 10^{-4}$		ITAE $\times 10^{-4}$	
	Speed	Current	Speed	Current	Speed	Current	Speed	Current
PID	36.17	2482	2975	7707	2952	50750	33380	400200
PID*n*	10.65	10270	1028	39340	37.3	93600	6114	527300
FOPID	19.58	23420	1785	65460	1223	332600	17080	997000
FOPI(1 +PID*n*)	6.995	7077	624.4	39900	10.6	103400	2010	605500

Table 14
Transient response specifications with delay time in case 2.

Controller	T_r	T_s	T_p	OS
PID	11.9238	26.2255	29.8479	0.27688
PID*n*	3.3325	15.6756	6.9318	16.2995
FOPID	3.0378	28.1753	8.3441	23.696
FOPI(1 +PID*n*)	3.1794	8.8723	6.5294	4.8496

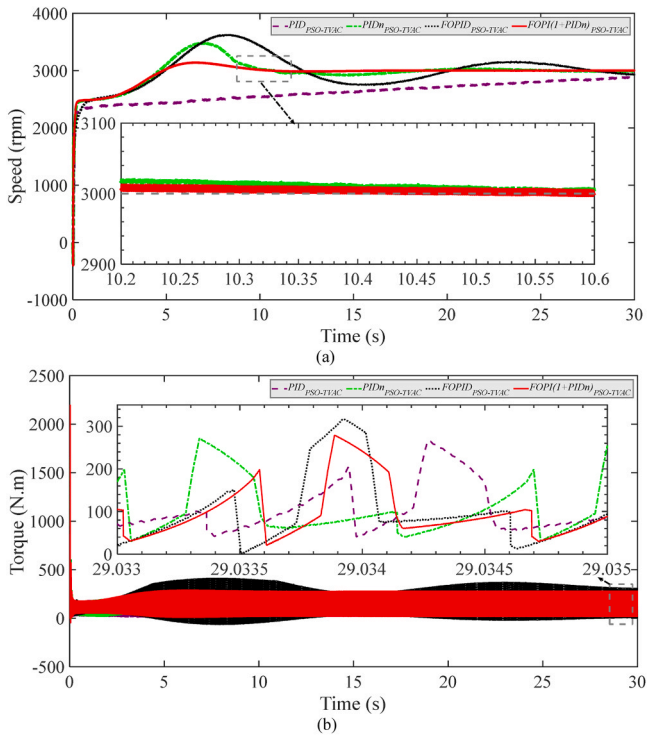


Fig. 9. Time response of (a) Speed, (b) Total torque, with time-delay for proposed and other controllers in Case 2.

following and tracking the reference speed, respectively. Also, the values of the transient response specifications of the system are listed in Table 6 The values of this table show well that the proposed controller has a faster performance compared to other controllers. Additionally, the Fig. 6(b) shows well that at the reference speed, the proposed controller has the lowest torque ripple among other controllers. The Table 7 shows the values of the torque ripples. Fig. 6(c) shows the output current for one phase of the SRM with different controllers. The time domain evaluation indicators for the internal and external controller are listed in Table 8. It is found that in the proposed controller, the numerical values of the error are better.

5.1.1. *No load with time-delay non-linearity*

Complications in managing systems arise from factors like time-delays non-linearity by power line interference or SRM malfunctions. In this scenario, it is presumed that the control system's stimulation signal experiences a 20 ms delay on outer controller. The 20 ms delay introduced in this study represents a conservative approximation of cumulative digital execution, sampling, and PWM update delays commonly observed in practical SRM drive systems. The objective is to evaluate controller robustness under a significant fixed delay disturbance rather than to perform a full parametric delay sweep. This value was selected to represent a non-negligible worst-case latency condition. As shown in the Fig. 7(a), the proposed controller has a better performance in reaching the reference speed. The controller of PID*n*, PID and FOPID are ranked next. Transient response values are shown in the Table 9.

Table 15
Comparison of the torque values and torque ripples in case 2.

Controller	T_{max}	T_{min}	T_{avg}	$\%T_{ripple}$
PID	265.86	39.49	104.13	217.39
PID*n*	271.85	29.81	104.00	232.47
FOPID	316.76	0.96	98.41	320.89
FOPI(1 +PID*n*)	278.90	21.04	98.52	261.73

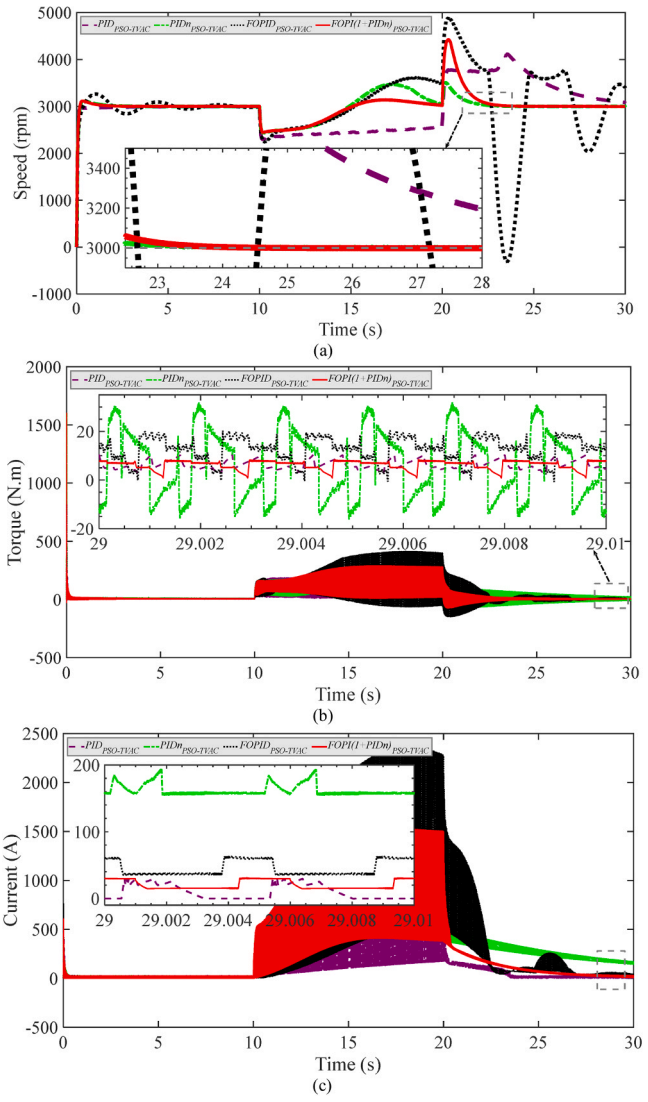


Fig. 10. Time response of (a) Speed, (b) Total torque, (c) Phase current for proposed and other controllers in Case 3.

Fig. 7(b) shows the SRM torque curve, in which the performance of the proposed controller is acceptable. It should be noted that the proposed controller has a very good torque ripple at the reference speed, while other controllers have not reached the reference speed. The torque ripple values are in the Table 10.

5.2. *Case 2: static load*

Since motors don't always operate under ideal conditions, a load torque of 100 N.m is applied to the SRM to assess the controllers' performance in this scenario. Fig. 8(a) illustrates the speed response while imposing a 100 N.m load on the SRM. Carefully in the Fig. 8(a), it is clear

Table 16
Comparison of the torque values and torque ripples in case 3.

Controller	T_{max}	T_{min}	T_{avg}	$\%T_{ripple}$
PID	10.37	2.77	6.24	121.75
PID*n*	32.10	-16.20	6.28	769.14
FOPID	20.29	-0.70	12.70	165.36
FOPI(1 +PID*n*)	8.34	0.83	6.28	119.59

Table 17
Time-based indicators illustrating the dynamic response of the SRM in case 3.

Controller	ISE × 10^4		IAE × 10^4		ITSE × 10^4		ITAE × 10^4	
	Speed	Current	Speed	Current	Speed	Current	Speed	Current
PID	48.35	250.25	2910	4645	899.6	4390	54470	80080
PID*n*	12	7251	1065	22200	149.7	104500	15180	371500
FOPID	127.1	11390	3930	28270	2794	199100	79510	496900
FOPI(1 +PID*n*)	16.07	2630	1032	15130	256.6	40730	15660	246800

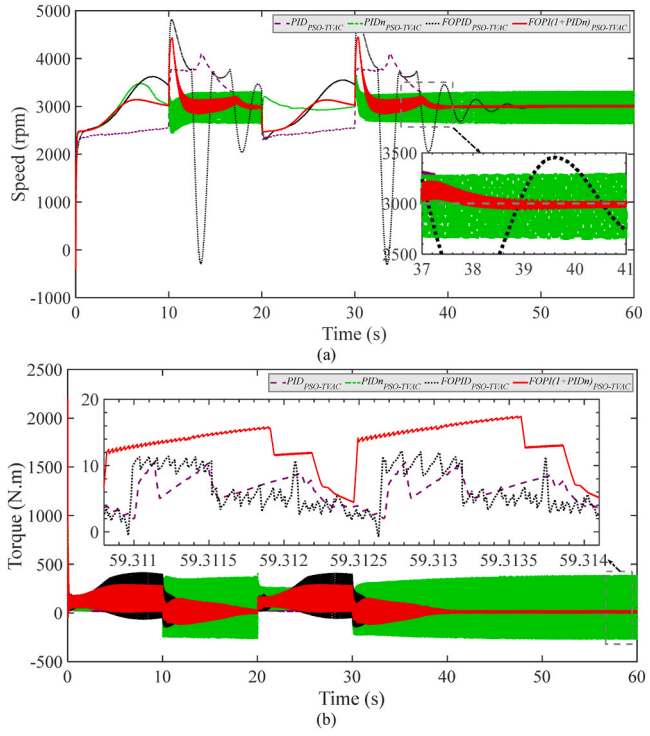


Fig. 11. Time response of (a) Speed, (b) Total torque, with time-delay for proposed and other controllers in Case 3.

that the proposed controller tracks the reference speed in less time compared to other controllers. The transient response characteristic values of the system are listed in Table 11. The values of this table show well that the proposed controller has the lowest settling time with a value of 8.99 s. These parameters show the advantage of the proposed controller in faster response. The torque ripple values are in the Table 12. An impressive benefit of the proposed controller is its very good and acceptable torque ripple value at the reference speed. Although the speed of SRM in other controllers does not reach the reference speed, the torque has more ripple than the FOPI(1 +PID*n*) controller. The Fig. 8(b) and 8(c) show the torque and current of the SRM in case 2. Table 13 presents the time domain assessment metrics for both the internal and external controllers. The results indicate that the proposed controller exhibits superior numerical values for the error of the external speed controller.

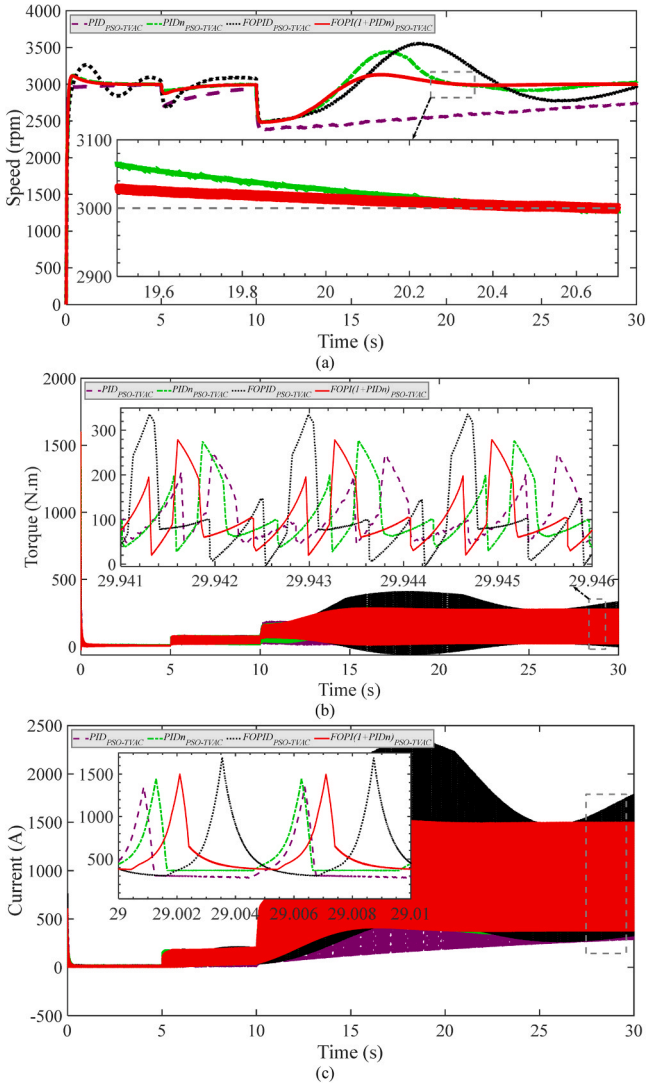


Fig. 12. Time response of (a) Speed, (b) Total torque, (c) Phase current for proposed and other controllers in Case 4.

5.2.1. *Static load with time-delay non-linearity*

In this scenario, it is assumed that the excitation signal of the control system experiences a delay of 20 ms in the external controller and a load of 100 N.m is applied to the SRM. In this operation, the proposed

Table 18
Comparison of the torque values and torque ripples in case 3.

Controller	T_{max}	T_{min}	T_{avg}	$\%T_{ripple}$
PID	10.58	1.05	6.29	151.52
PID*n*	352.37	-137.21	115.70	423.15
FOPID	12.24	-1.31	6.27	216.06
FOPI(1 +PID*n*)	16.91	2.99	14.94	93.172

Table 19
Comparison of the torque values and torque ripples in case 4.

Controller	T_{max}	T_{min}	T_{avg}	$\%T_{ripple}$
PID	250.61	43.04	107.73	192.68
PID*n*	277.21	27.99	106.16	234.75
FOPID	336.18	-4.88	107.40	317.57
FOPI(1 +PID*n*)	279.09	19.79	106.19	244.12

Table 20
Time-based indicators illustrating the dynamic response of the SRM in case 4.

Controller	ISE × 10^4		IAE × 10^4		ITSE × 10^4			ITAE × 10^4
	Speed	Current	Speed	Current	Speed	Current	Speed	Current
PID	30.27	1211	2546	12510	491.7	28540	44130	274400
PID*n*	9.491	8157	1012	28720	115.3	131900	14250	528900
FOPID	16.54	15660	1752	43460	239.3	309500	27090	872100
FOPI(1 +PID*n*)	6.23	4825	658.4	27240	60.24	95170	7621	541700

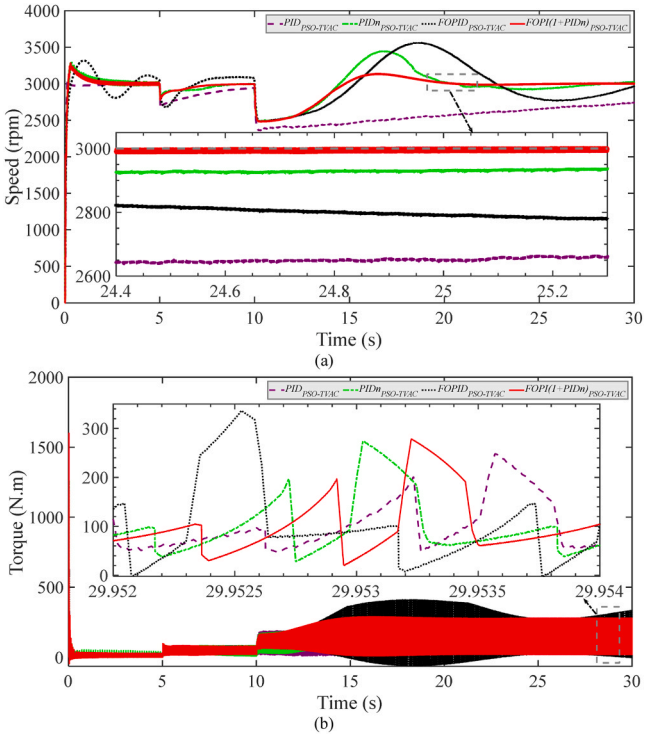


Fig. 13. Time response of (a) Speed, (b) Total torque, with time-delay for proposed and other controllers in Case 4.

Table 21
Comparison of the torque values and torque ripples in case 4.

Controller	T_{max}	T_{min}	T_{avg}	$\%T_{ripple}$
PID	248.26	46.84	100.89	199.65
PID*n*	274.02	27.85	99.32	247.87
FOPID	336.50	-4.40	98.74	345.23
FOPI(1 +PID*n*)	278.45	20.30	102.65	251.48

controller tracks the reference speed with a very low overshoot and extremely low settling time compared to other controllers. The values are in the Table 14 The Fig. 9(a) shows that the controllers of PID*n*, FOPID and PID have a slower response than FOPI(1 +PID*n*) in tracking the reference speed. Fig. 9(b) shows the torque in this scenario. The torque ripple values in the Table 15 show that the proposed controller is well capable of controlling the torque ripple at the reference speed.

5.3. Case 3: dynamic load

In this section, a dynamic load of 100 N.m is applied into the SRM at $t = 10$s and removed from the SRM at $t = 20$s. Fig. 10(a) shows the performance of the proposed controller in this scenario. As can be seen from Fig. 10(a), the proposed controller shows less speed drop than other controllers when the load is applied, and when the applied load is removed, the proposed controller shows its ability to track the reference speed well. FOPID and PID controllers are weak in reaching the

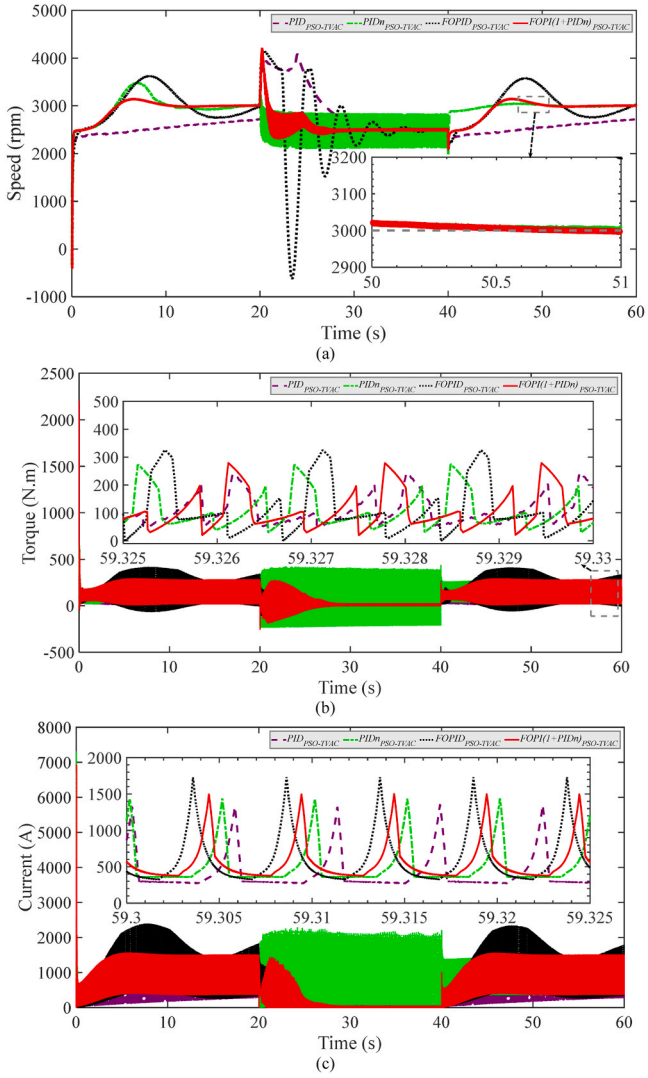


Fig. 14. Time response of (a) Speed, (b) Total torque, (c) Phase current for proposed and other controllers in Case 5.

reference speed within the defined time period. The controller FOPI (1 +PID*n*) shows impressive performance in torque ripple reduction. FOPI(1 +PID*n*), PID, FOPID and PID*n* controllers with torque ripple values of 119.59, 121.75, 165.36, and 769.14 show their ability to reduce the torque ripple, respectively. Table 16 and Fig. 10(b) and 10(c) show the torque ripple values and torque, current curve of the SRM in this scenario. Time domains values are in Table 17.

5.3.1. Dynamic load with time-delay non-linearity

Time delay with dynamic load of 100 N.m is applied into the SRM at $t = 10$s and removed from the SRM at $t = 20$s. In this case, 60 s simulation time is chosen to show the efficiency of the controllers and to

Table 22
Comparison of the torque values and torque ripples in case 5.

Controller	T_{max}	T_{min}	T_{avg}	$\%T_{ripple}$
PID	245.43	50.42	108.70	179.41
PID*n*	274.37	29.08	106.09	231.22
FOPID	325.81	-2.34	106.78	307.31
FOPI(1 +PID*n*)	279.48	19.50	106.44	244.24

Table 23
Sensitivity analysis parameters for the SRM under uncertain operating conditions.

Parameter	Increased by 20%	decreased by 20%
R_s (Ω)	0.06	0.04
Inertia (kg.m^2)	0.06	0.04
Friction (N.m.s)	0.024	0.016

Table 24
Dynamic response of SRM under stator resistance variations.

Parameter	Rate of change	Controller	T_r	T_s	T_P	OS
R_s	-20%	PID	0.10041	0.5486	31.547	0.0125
		PID*n*	0.13797	0.1074	0.5015	6.1745
		FOPID	0.17054	6.2154	0.9048	10.201
		FOPI (1+PID*n*)	0.09941	0.9054	0.1475	3.9974
R_s	+20%	PID	0.98542	0.3145	27.101	0.0254
		PID*n*	0.84125	0.6014	0.7415	6.0874
		FOPID	0.50214	3.5874	0.5651	13.810
		FOPI (1+PID*n*)	0.15223	0.8147	0.0174	3.9751

reach their steady-state error to zero. In the Fig. 11(a) well, the time of the controllers reaching the reference speed is shown, and the proposed controller provides very favorable results by surpassing other controllers. Fig. 11(b) torque diagram It shows the SRM in this scenario, and it is clear that the ripple FOPI(1 +PID*n*) controller has much less torque than other controllers. The values of the ripple torque in the Table 18 have come, which confirms the correctness of this claim.

5.4. Case 4: stepwise load increase

In this scenario, the load is increased in steps to investigate the behavior of the SRM in this state. In the first step, a load of 50 N.m is applied to the motor at $t = 5$s. In the second step, it increases to 100 N.m at $t = 10$s. In Fig. 12(a), the behavior of the FOPI(1 +PID*n*) controller shows that, as expected, the speed drop is less than other controllers when applying a high load. Also, tracking the reference speed in a short period of time and less steady-state error is distinguishing features of the proposed controller. The torque ripple values reported in Table 19 show that in the proposed controller, even though the SRM is at its maximum speed, the ripple torque is satisfactory. The Fig. 12(b) and 12(c) show the torque and current of the SRM in case 4. Also, the time domain values presented in Table 20 demonstrate that the performance of the proposed controller surpasses that of the other controllers.

To avoid ambiguity, it is important to emphasize that the error-based indices ISE, IAE, ITSE, and ITAE are fully meaningful and directly comparable as long as all controllers operate under the same load profile and excitation within each simulation case. Since each case in this study applies identical conditions to all controllers, the indices reported in Tables 8, 13, 17, and 20 provide a fair and consistent assessment of performance for every scenario. Furthermore, because the SRM drive maps the controller output directly to phase excitation, the integrated control effort is inherently reflected in the resulting current waveform. Therefore, the current-related indices already quantify the relative control-signal energy across controllers, and no additional duplicated energy metrics are required.

5.4.1. Stepwise load increase with time-delay non-linearity

As Fig. 13(a), with a time delay, the load increases step by step. The load applied to the system in the first and second stages can prove the efficiency of the FOPI(1 +PID*n*) controller. In these two stages, despite the time delay, the reduction of the SRM speed from the no-load speed is less than other controllers. Also, the proposed controller shows its ability to reach the reference speed in the Fig. 13(a). Also, the SRM torque is shown in Fig. 13(b). The torque ripple values in Table 21 indicate that, even while the SRM operates at the reference speed, it maintains an acceptable torque ripple.

5.5. Case 5: complicated operation

In this scenario, a very complex and critical operation is provided for the SRM in order to evaluate the operation of the controller in this rare condition. This stage is defined in three steps as follows:

- T = 100 N.m at $t = 0$s until $t = 20$s and reference speed 3000 r.p.m
- T = 0 N.m at $t = 20$s until $t = 40$s and decrease reference speed 2500 r.p.m
- T = 100 N.m at $t = 40$s until $t = 60$s and increase reference speed 3000 r.p.m

As shown in the Fig. 14(a) it is clear that the proposed controller with more flexible performance than other controllers can guarantee the reliable operation of the SRM in abnormal operations. Fig. 14(b)

Table 26
Dynamic response of SRM under friction variations.

Parameter	Rate of change	Controller	T_r	T_s	T_p	OS
Friction	-20%	PID	1.5741	1.5987	0.8541	0.6954
		PID*n*	1.2527	0.9653	0.3214	0.8574
		FOPID	1.8791	3.7451	1.7412	0.9415
		FOPI (1+PID*n*)	1.7412	1.2117	0.6521	0.0841
Friction	+20%	PID	0.9141	1.7412	0.3147	0.8745
		PID*n*	0.8452	1.5214	0.7416	0.6324
		FOPID	0.6325	1.2324	1.0546	0.8868
		FOPI (1+PID*n*)	0.0841	0.8745	0.2207	0.1087

Table 25
Dynamic response of SRM under inertia variations.

Parameter	Rate of change	Controller	T_r	T_s	T_p	OS
Inertia	-20%	PID	0.09147	0.3412	24.1254	0.00954
		PID*n*	0.11257	0.0914	0.32012	1.74157
		FOPID	0.14512	4.8541	0.52149	2.8741
		FOPI(1+PID*n*)	0.10147	0.0847	0.28541	2.4141
Inertia	+20%	PID	0.93541	1.9854	15.4120	0.0041
		PID*n*	0.71542	1.7125	0.15478	2.0741
		FOPID	1.47126	5.0179	0.34153	4.7814
		FOPI(1+PID*n*)	0.44125	1.0285	0.19841	0.0248

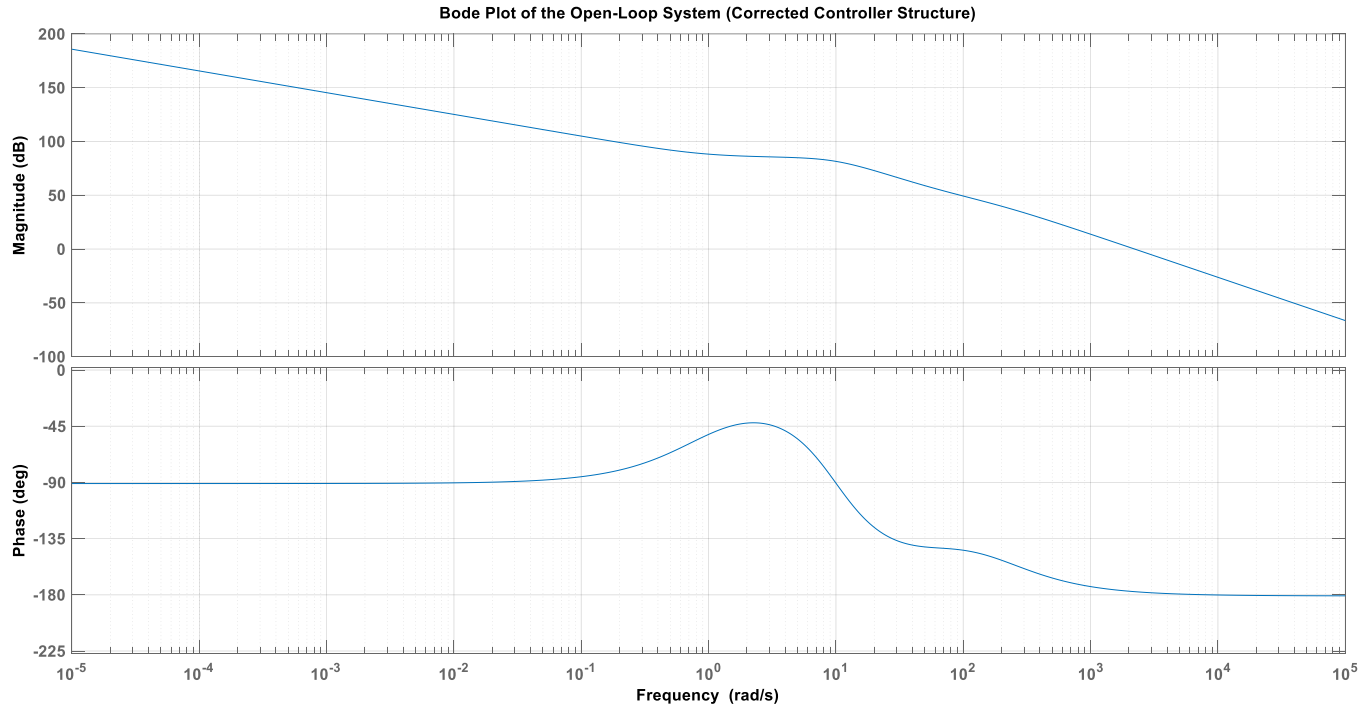


Fig. 15. Bode plot of open loop for linear SRM structure.

illustrates the SRM torque during a period when the motor operates at the reference speed. Unlike other controllers that cause the motor to run below the reference speed, this controller ensures the motor achieves the desired torque. Fig. 14(c) shows the output current for one-phase of the SRM with different controllers. The values of the torque ripple are in the Table 22.

5.6. Case 6: sensitivity analysis

In this scenario, a comprehensive sensitivity analysis was conducted to evaluate the robustness of the FOPI(1 +PIDn) controller for the SRM under uncertain operating conditions. Table 23 show values of parameters for this scenario.

As shown in Table 24, Table 25, and Table 26, the proposed FOPI (1+PIDn) controller demonstrated superior performance compared to PID, PIDn, and FOPID controllers. It maintained reliable operation and exhibited lower dynamic response values under these uncertain conditions. While other controllers struggled to keep the motor running at the desired efficiency, the proposed controller ensured better adaptability, stability, and torque accuracy across all variations.

5.7. Stability and robustness analysis

A theoretical stability analysis was performed to validate the proposed FOPI(1+PIDn) controller. The high-fidelity model developed in Simulink incorporates the highly non-linear dynamics of the SRM, along with the discontinuous, switching-based logic of the power converter and hysteresis control. Standard linearization techniques are not effective for such complex systems, as a well-defined linear equivalent cannot be easily extracted. Therefore, a standard two-model methodology is employed. This approach uses a nominal linear model for the theoretical stability analysis, and the high-fidelity non-linear model for performance validation. To conduct the theoretical analysis, the SRM plant was represented by a nominal Second-Order Plus Time-Delay (SOPTD) model, which is a standard structure for approximating the dominant dynamics of electromechanical systems. The transfer function for this nominal plant model, $G_p(s)$, is defined as:

$$G_p(s) = \frac{K.e^{-\theta s}}{\tau^2 s^2 + 2\xi\tau s + 1} \tag{17}$$

The parameters of this model are estimated to align with the dynamic response characteristics observed in the no-load simulation results presented in Fig. 6a and Table 6. The gain (K), was set to 3000 to match the system's steady-state speed. The time constant (τ), was set to 0.1 s to reflect the measured rise time of 0.096 s. The damping ratio ξ, was chosen as 0.8 to represent the low overshoot of 3.88% shown in the simulation results. Finally, a minor delay (θ), of 0.01 s was included to account for computational and hardware latencies. The stability of the closed-loop system is then evaluated using frequency-domain analysis. A Bode plot of the open-loop transfer function, $L(s) = G_c(s)G_p(s)$, was generated in Fig. 15.

The analysis revealed a gain margin of 14.91 dB and a phase margin of 2.52 °. For a standard linear system, such a critically low phase margin would predict a poorly damped response characterized by significant overshoot and prolonged oscillations. Also, the stability of the proposed FOPI(1 +PIDn) controller is further justified by considering the bounded-input bounded-output (BIBO) stability criteria for fractional-order systems. Since the fractional order λ is within the range (0, 2), the system's poles in the complex s-plane remain in the left-half plane, fulfilling the condition $|arg(spec(A))| > \frac{\lambda\pi}{2}$ for the linearized sub-models of the SRM.

To validate the controller's true performance, it is tested on the high-fidelity non-linear SRM model in Simulink, which incorporates the complex dynamics ignored by the simplified linear model. Contrary to the prediction of the linear analysis, the simulation results presented in Section 5 demonstrate that the proposed controller achieves excellent performance, exhibiting minimal overshoot (3.88%) and a rapid settling time. This disparity highlights the remarkable robustness of the FOPI (1+PIDn) design. The controller is so effective that it actively compensates for the severe non-linearities of the true plant, delivering superior performance that overcomes the limitations predicted by the nominal linear model. Therefore, the simulation results serve as the definitive validation of the controller's stable and highly effective operation in a realistic environment.

6. Concluding remarks and future directions

This study presents the development of a novel FOPI(1+PID*n*) multistage controller, designed to address the persistent challenges of speed control and torque ripple reduction in SRMs. The proposed controller's performance was optimized using the PSO-TVAC algorithm, resulting in significant improvements over traditional control methods. Key findings demonstrate that the FOPI(1+PID*n*) controller achieves a notable 57% reduction in the CF value compared to other controllers, along with average reductions of 65% in the ISE index and 45% in the ITSE index in the outer speed controller across six different scenarios. These improvements translate into enhanced dynamic response characteristics, including better rise time (T_r), settling time (T_s), peak time (T_p), and overshoot (OS). Additionally, the controller effectively minimizes torque ripple while achieving super-fast tracking of the reference speed, solidifying its superiority over traditional PID, PID*n*, and FOPID controllers.

The simplicity of the FOPI(1+PID*n*) controller, combined with its exceptional performance, makes it a highly desirable choice for complex SRM control tasks. Its robust and stable operation under various challenging conditions underscores its potential for broad applications in industrial motor control.

It is important to acknowledge the limitations of this study. The evaluations were conducted primarily in simulated environments, which, although controlled, may not fully capture the complexities of real-world applications. Factors such as electrical noise, component tolerances, and practical implementation challenges could affect the controller's performance outside the simulation environment. Additionally, the study's focus on SRMs limits the generalizability of the findings to other motor types. The specific characteristics of SRMs were central to this research, and the controller's effectiveness in different motor systems remains untested. Furthermore, the optimization process relied on the PSO-TVAC algorithm, and exploring alternative or hybrid optimization techniques might reveal additional performance benefits.

Looking ahead, several avenues for future research are suggested. Implementing the FOPI (1+PID*n*) controller in real-time control systems and conducting hardware in the loop (HIL) simulations could provide valuable insights into its practical viability and robustness. Additionally, extending the application of this controller to other types of electric motors, such as PMSMs or IMs, could broaden its applicability. Further exploration of more advanced optimization methods, including genetic algorithms or machine learning-based approaches, could also enhance the controller's adaptability and performance in diverse operating conditions. Finally, long-term studies focusing on the durability and reliability of the controller under continuous operation would be crucial for ensuring its effectiveness in real-world industrial applications. Also, peak-to-peak ripples are used as the primary comparison metric due to its relevance in control-oriented evaluation, harmonic-domain analysis may provide additional insight into ripple frequency components and will be investigated in future studies.

CRediT authorship contribution statement

Mostafa Jabari: Writing – original draft, Visualization, Supervision, Methodology, Investigation, Formal analysis, Data curation, Conceptualization. **Serdar Ekinci:** Writing – original draft, Visualization, Validation, Supervision, Project administration, Methodology, Investigation, Formal analysis, Conceptualization. **Davut Izci:** Writing – review & editing, Visualization, Validation, Supervision, Project administration, Methodology, Data curation, Conceptualization. **Mohit Bajaj:** Writing – review & editing, Visualization, Validation, Supervision, Resources, Methodology, Investigation, Formal analysis. **Vojtech Blazek:** Writing – review & editing, Visualization, Validation, Supervision, Resources, Project administration, Methodology, Funding acquisition, Formal analysis. **Lukas Prokop:** Writing – review & editing, Visualization, Validation, Supervision, Project administration, Methodology, Funding acquisition, Formal analysis.

Funding

This research is funded by European Union under the REFRESH—Research Excellence For Region Sustainability and High-Tech Industries Project via the Operational Programme Just Transition under Grant CZ.10.03.01/00/22_003/0000048; in part by the National Centre for Energy II and ExPEDite Project a Research and Innovation Action to Support the Implementation of the Climate Neutral and Smart Cities Mission Project TN02000025; and in part by ExPEDite through European Union's Horizon Mission Programme under Grant 101139527.

Declaration of Competing Interest

The authors declare that they have no known competing financial interests or personal relationships that could have appeared to influence the work reported in this paper.

Acknowledgements

This research is funded by European Union under the REFRESH—Research Excellence For Region Sustainability and High-Tech Industries Project via the Operational Programme Just Transition under Grant CZ.10.03.01/00/22_003/0000048; in part by the National Centre for Energy II and ExPEDite Project a Research and Innovation Action to Support the Implementation of the Climate Neutral and Smart Cities Mission Project TN02000025; and in part by ExPEDite through European Union's Horizon Mission Programme under Grant 101139527. The authors would like to express their sincere gratitude to Stanislav Misak for his exceptional supervision, project administration, and overall guidance throughout the course of this project. His expertise and support were instrumental to its success.

Appendix 1. Design parameter specifications used in this study

Rated voltage	**240 V_{dc}**	K_{I-C}	**7.010**
Rated power	60 kW	K_{D-C}	0
Rated speed	3000 r.p.m	K_{PP-S}	3.510
Turn off angle	75°	K_{II-S}	4.030
Turn on angle	45°	K_{PP-C}	20
Stator resistance	0.05 Ω	K_{II-C}	12.880
Inertia	0.05 kg.m^2	U_{B-H}	1.979
Friction	0.02 N.m.s	L_{B-H}	-3.405
K_{P-S}	0.014	λ_S	0.010
K_{I-S}	1.419	λ_C	0.04
K_{D-S}	0.043	N_S	183.611
K_{P-C}	20	N_C	747.520

Data availability

Data will be made available on request.

References

Abualigah, Laith, Izci, Davut, Ekinci, Serdar, Zitar, Raed, 2024b. Optimizing aircraft pitch control systems: a novel approach integrating artificial rabbits optimizer with PID-F controller. Int. J. Robot. Control Syst. 4 (1).

Abualigah, Laith, Ekinci, Serdar, Izci, Davut, 2024a. Aircraft pitch control via filtered proportional-integral derivative controller design using sinh cosh optimizer. Int. J. Robot. Control Syst. 4 (2).

Agajie, T.F., et al., 2023. Optimal sizing and power system control of hybrid solar PV-biogas generator with energy storage system power plant. Sustainability 15 (7), 5739.

Ahmad, S.S., Narayanan, G., 2016. Linearized modeling of switched reluctance motor for closed-loop current control. IEEE Trans. Ind. Appl. 52 (4), 3146–3158.

Al Samman, Fathia Moh, Abdul Khaliq, Wajiha, Hilali, Shreefa O., Niazi, Azmat Ullah Khan, Smerat, Aseel, 2025. Adaptive neural network based leader-following consensus control for a class of second-order nonlinear multi-agent systems: F. Al Samman et al. Sci. Rep. 15 1, 36040.

Al-Amyal, F., Számel, L., Hamouda, M., 2023. An enhanced direct instantaneous torque control of switched reluctance motor drives using ant colony optimization. Ain Shams Eng. J. 14 (5), 101967.

Aribowo, Widi, Rahmadian, Reza, Widyartono, Mahendra, Wardani, Ayusta Lukita, Prapanca, Aditya, Abualigah, Laith, 2024. Controlling parameters proportional integral derivative of DC motor using a gradient-based optimizer. Int. J. Power Electron. Drive Syst. (IJPEDS) 15 (2), 696–703. https://doi.org/10.11591/ijpeds.v15.i2.pp696-703.

Bergies, S., Su, S.-F., Elsisi, M., 2022. Model predictive paradigm with low computational burden based on dandelion optimizer for autonomous vehicle considering vision system uncertainty. Mathematics 10 (23), 4539.

Bogusz, P., Korkosz, M., Prokop, J., Daraż, M., 2021. Analysis performance of SRM based on the novel dependent torque control method. Energies 14 (24), 8203.

Cai, H., Wang, H., Li, M., Shen, S., Feng, Y., Zheng, J., 2018. Torque ripple reduction for switched reluctance motor with optimized PWM control strategy. Energies 11 (11), 3215.

Dang, X., Shi, Y., Peng, H., 2020. Torque–flux linkage recurrent neural network adaptive inversion control of torque for switched reluctance motor. IET Electr. Power Appl. 14 (9), 1612–1623.

Divandari, M., Rezaie, B., Noei, A.R., 2019. Speed control of switched reluctance motor via fuzzy fast terminal sliding-mode control. Comput. Electr. Eng. 80, 106472.

Ekinci, Serdar, Izci, Davut, Almomani, Mohammad H., Saleem, Kashif, Zitar, Raed Abu, Smerat, Aseel, Snasel, Vaclav, Ezugwu, Absalom E., Abualigah, Laith, 2025. Advanced control parameter optimization in DC motors and liquid level systems. Sci. Rep. 15 (1), 1394.

El-Kharahi, E., El-Dessouki, M., Lindh, P., Pyrhönen, J., 2015. Toward including the effect of manufacturing processes in the pre-estimated losses of the switched reluctance motor. Ain Shams Eng. J. 6 (1), 121–131.

Elsisi, M., 2024. Optimal design of adaptive model predictive control based on improved GWO for autonomous vehicle considering system vision uncertainty. Appl. Soft Comput. 158, 111581.

Elsisi, M., Zaini, H.G., Mahmoud, K., Bergies, S., Ghoneim, S.S., 2021. Improvement of trajectory tracking by robot manipulator based on a new co-operative optimization algorithm. Mathematics 9 (24), 3231.

Elsisi, M., Altius, M., Su, S.-F., Su, C.-L., 2023. Robust Kalman filter for position estimation of automated guided vehicles under cyberattacks. IEEE Trans. Instrum. Meas. 72, 1–12.

Elsisi, M., Ali, M.N., Aljohani, T.M., Sharawy, M., 2024. A new variable step fuzzy logic control technique for minimum emission point tracking of ship microgrid. IEEE Trans. Transp. Electrification.

Fang, G., Scalcon, F.P., Xiao, D., Vieira, R.P., Gründling, H.A., Emadi, A., 2021. Advanced control of switched reluctance motors (SRMs): a review on current regulation, torque control and vibration suppression. IEEE Open J. Ind. Electron. Soc. 2, 280–301.

Gan, C., Wu, J., Sun, Q., Kong, W., Li, H., Hu, Y., 2018. A review on machine topologies and control techniques for low-noise switched reluctance motors in electric vehicle applications. IEEE Access 6, 31430–31443.

Gengaraj, M., Kalaivani, L., Rajesh, R., 2023. Investigation on torque sharing function for torque ripple minimization of switched reluctance motor: a flower pollination algorithm based approach. IETE J. Res. 69 (6), 3678–3692.

Gupta, Monika, Tiwari, P.M., Viral, R.K., Shrivastava, Ashish, Zneid, Basem Abu, Hunko, Iryna, 2025. Grid-connected PV inverter system control optimization using Grey Wolf optimized PID controller. Sci. Rep. 15 (1), 28869.

Hameed, H.S., Al Azze, Q., Hasan, M.S., 2023. Speed control of switched reluctance motors based on fuzzy logic controller and MATLAB/Simulink. Indones. J. Electr. Eng. Comput. Sci. 31 (2), 647–657.

Hu, K., Ye, J., Velni, J.M., 2019. Sliding mode current control of mutually coupled switched reluctance machines using a three-phase voltage source converter. 2019 IEEE Energy Conversion Congress and Exposition (ECCE). IEEE, pp. 1776–1781.

Hu, K., Guo, L., Ye, J., 2020. Model predictive current control of mutually coupled switched reluctance machines using a three-phase voltage source converter. 2020 IEEE Applied Power Electronics Conference and Exposition (APEC). IEEE, pp. 704–710.

Huang, H.-N., Hu, K.-W., Wu, Y.-W., Jong, T.-L., Liaw, C.-M., 2016. A current control scheme with back EMF cancellation and tracking error adapted commutation shift for switched-reluctance motor drive. IEEE Trans. Ind. Electron. 63 (12), 7381–7392.

Hussein, Ahmad MohdAziz, Alomari, Saleh Ali, Almomani, Mohammad H., Zitar, Raed Abu, Migdady, Hazem, Smerat, Aseel, Snasel, Vaclav, Abualigah, Laith, 2025. A hybrid PSO-GCRA framework for optimizing control systems performance. Int. J. Robot. Control Syst. 5 1.

Izci, Davut, Rizk-Allah, Rizk M., Snášel, Václav, Ekinci, Serdar, Migdady, Hazem, Daoud, Mohammad Sh, Altalhi, Maryam, Abualigah, Laith, 2024a. Refined sinh cosh optimizer tuned controller design for enhanced stability of automatic voltage regulation. Electr. Eng. 106 (5), 6003–6016.

Izci, Davut, Abualigah, Laith, Can, Özay, Andiç, Cenk, Ekinci, Serdar, 2024b. Achieving improved stability for automatic voltage regulation with fractional-order PID plus double-derivative controller and mountain gazelle optimizer. Int. J. Dyn. Control 12 (7), 2550–2565.

Izci, Davut, Ekinci, Serdar, Rizk-Allah, Rizk M., Alribdi, Nada Ibrahim, Smerat, Aseel, Alzahrani, Ahmed, Alwadain, Ayed, Snasel, Vaclav, Abualigah, Laith, 2025. Master–Slave Architecture Enhanced and Improved GBO Tuned Cascaded PI-PDN Controller for Speed Regulation of DC Motors. Optim. Control Appl. Methods.

Jabari, M., et al., 2025a. An advanced PID tuning method for temperature control in electric furnaces using the artificial rabbits optimization algorithm. Int. J. Dyn. Control 13 (5), 1–15.

Jabari, M., Rad, A., 2024. Optimization of speed control and reduction of torque ripple in switched reluctance motors using metaheuristic algorithms based PID and FOPID controllers at the edge. Tsinghua Sci. Technol.

Jabari, M., Ekinci, S., Izci, D., Bajaj, M., Blazek, V., Prokop, L., 2025a. Efficient pressure regulation in nonlinear shell-and-tube steam condensers via a Novel TDn (1+ PIDn) controller and DCSA algorithm. Sci. Rep. 15 (1), 2090.

Jabari, M., Izci, D., Ekinci, S., Bajaj, M., Blazek, V., Prokop, L., 2025a. Hybrid adaptive ant lion optimization with traditional controllers for driving and controlling switched reluctance motors to enhance performance. Sci. Rep. 15 (1), 12898.

Jabari, Mostafa, Ekinci, Serdar, Izci, Davut, Zitar, Raed Abu, Migdady, Hazem, Smerat, Aseel, Abualigah, Laith, 2025b. An advanced pid tuning method for temperature control in electric furnaces using the artificial rabbits optimization algorithm. Int. J. Dyn. Control 13 (5), 1–15.

Jan, Farman Ullah, Badar, Rabiah, Al-Shamayleh, Ahmad Sami, Uehara, Akie, Senjyu, Tomonobu, Akhunzada, Adnan, 2025. Soft computing based damping controllers with online parameters tuning for stability enhancement of power systems. IEEE Access.

Kotb, H., Yakout, A.H., Attia, M.A., Turky, R.A., AboRas, K.M., 2022. Speed control and torque ripple minimization of SRM using local unimodal sampling and spotted hyena algorithms based cascaded PID controller. Ain Shams Eng. J. 13 (4), 101719.

Kumar, M.N., Chidanandappa, R., 2024. Particle swarm optimization technique for speed control and torque ripple minimization of switched reluctance motor using PID and FOPID controllers. Int. J. Inf. Technol. 16 (2), 1185–1201.

Liu, Di, Fan, Yunsheng, Liu, Jian, Wang, Guofeng, Sheng, Linhao, 2024. Robust deadbeat predictive current control for unipolar sinusoidal excited SRM with multi-parameter mismatch compensation. Sci. Rep. 14 (1), 23746.

Mahalakshmi, G., Kanthalakshmi, S., 2022. Design of Iterative Learning Controller for Switched Reluctance Motor with Least Torque Ripple. In: 2022 8th International Conference on Advanced Computing and Communication Systems (ICACCS), 1. IEEE, pp. 299–304.

Martin, G., Kumar, C.A., 2021. Novel bio-inspired algorithm for speed control and torque ripple reduction of switched reluctance motor in aerospace application. J. Electr. Eng. Technol. 16 (3), 1359–1374.

Memon, A.A., Shaikh, M.M., Bukhari, S.S.H., Ro, J.-S., 2020. Look-up data tables-based modeling of switched reluctance machine and experimental validation of the static torque with statistical analysis. J. Magn. 25 (2), 233–244.

Memon, A.A., Bukhari, S.S.H., Hao, C., 2023. Switched reluctance motoring and generating operation in single pulse, current chopping and voltage PWM modes. Electr. Eng. 105 (5), 2817–2823.

Mohamed, M.A.E., Mohamed, S.M.R., Saied, E.M.M., Elsisi, M., Su, C.-L., Hadi, H.A., 2022. Optimal energy management solutions using artificial intelligence techniques for photovoltaic empowered water desalination plants under cost function uncertainties. Ieee Access 10, 93646–93658.

Mohanraj, Deepak, Devakirubakaran, S., Balachandran, Praveen Kumar, 2024. An improved finite set model predictive control of SRM drive based on a voltage vectors strategy for low torque ripple. Heliyon 10 (20).

Nimisha, K., Senthilkumar, R., 2018. Optimal tuning of PID controller for switched reluctance motor speed control using particle swarm optimization. 2018 International Conference on Control, Power, Communication and Computing Technologies (ICCPCCT). IEEE, pp. 487–491.

Oshaba, A., Ali, E., Elazim, S.Abd, 2015. ACO based speed control of SRM fed by photovoltaic system. Int. J. Electr. Power Energy Syst. 67, 529–536.

Oubouaddi, H., Brouri, A., Ouannou, A., 2022. Speed control of Switched Reluctance Machine using fuzzy controller and neural network. 2022 International Conference on Intelligent Systems and Computer Vision (ISCV). IEEE, pp. 1–6.

Pan, J., et al., 2017. Complimentary force allocation control for a dual-mover linear switched reluctance machine. Energies 11 (1), 23.
Peng, F., Ye, J., Emadi, A., 2015. A digital PWM current controller for switched reluctance motor drives. IEEE Trans. Power Electron. 31 (10), 7087–7098.
H.S.A. Rahnama, (n.d.) DESIGNING A PD-(1+ PI) CONTROLLER FOR LFC OF AN ENTIRELY RENEWABLE MICROGRID USING PSO-TVAC.
Ren, P., Zhu, J., Jing, Z., Guo, Z., Xu, A., 2022. Improved DITC strategy of switched reluctance motor based on adaptive turn-on angle TSF. Energy Rep. 8, 1336–1343.
Saha, N., Mishra, P.C., 2023. Modified whale algorithm-based optimization for fractional order concurrent diminution of torque ripple in switch reluctance motor for EV applications. Processes 11 (4), 1226.
Scalcon, F.P., Vieira, R.P., Gründling, H.A., 2022. Pso-based fast mechanical parameters estimation of switched reluctance motor drives. J. Control Autom. Electr. Syst. 33 (4), 1286–1293.
Senthil Murugan, L., Maruthupandi, P., 2020. Sensorless speed control of 6/4-pole switched reluctance motor with ANFIS and fuzzy-PID-based hybrid observer. Electr. Eng. 102, 831–844.
Shadhik, M., Senthil Kumaran, M., 2023. Meta heuristic optimization algorithm based rectifier control in switched reluctance generator. IETE J. Res. 1–23.
Shayeghi, H., Rahnama, A., 2022. Frequency regulation of a standalone interconnected AC microgrid using innovative multistage TDF(1+FOPI) controller. J. Oper. Autom. Power Eng. https://doi.org/10.22098/joape.2023.10668.1768.
Shayeghi, H., Rahnama, A., Bizon, N., 2023. TFODn-FOPI multi-stage controller design to maintain an islanded microgrid load-frequency balance considering responsive loads support. IET Gener. Transm. Distrib.
Shen, Xiaoning, Liu, Jianxing, Liu, Zhuang, Gao, Yabin, Leon, Jose I., Vazquez, Sergio, Wu, Ligang, Franquelo, Leopoldo G., 2024. Sliding-mode control of neutral-point-clamped power converters with gain adaptation. IEEE Trans. Power Electron. 39 (8), 9189–9201.
Song, X., Zhu, J., Ren, P., Lv, X., 2021. An improved fuzzy control for switched reluctance motor based on torque sharing function. 2021 6th International Conference on Automation, Control and Robotics Engineering (CACRE). IEEE, pp. 119–123.
Souza, D.A., de Mesquita, V.A., Reis, L.L., Silva, W.A., Batista, J.G., 2021. Optimal lqi and pid synthesis for speed control of switched reluctance motor using metaheuristic techniques. Int. J. Control Autom. Syst. 19, 221–229.
Sun, X., Diao, K., Lei, G., Guo, Y., Zhu, J., 2019. Direct torque control based on a fast modeling method for a segmented-rotor switched reluctance motor in HEV application. IEEE J. Emerg. Sel. Top. Power Electron. 9 (1), 232–241.
Sun, X., Zhu, Y., Cai, Y., Zhu, Z., Xiong, Y., 2023. Speed sensorless control of switched reluctance motors in full speed range based on inductance characteristics. IEEE Trans. Transp. Electrification.
Tepljakov, A., Tepljakov, A., 2017. FOMCON: fractional-order modeling and control toolbox. Fractional-order modeling and control of dynamic systems 107–129.
Turab, Nidal, Raghu, N., Choudhury, Satish, Zkear Abass, Ahmed, Roslin, S.Emalda, Kaur, Gaganjot, Pant, Ruby, Chauhan, Gauri, Khorasanikia Asl, Abdolreza, 2025. Adaptive sliding mode control for chaotic system synchronization using neural networks. Sci. Rep. 15 (1), 37547.
Uddin, W., Husain, T., Sozer, Y., Husain, I., 2016. Design methodology of a switched reluctance machine for off-road vehicle applications. IEEE Trans. Ind. Appl. 52 (3), 2138–2147.
Wang, S.-Y., Tseng, C.-L., Chien, S.-C., 2012. Adaptive fuzzy cerebellar model articulation control for switched reluctance motor drive. IET Electr. Power Appl. 6 (3), 190–202.
Wei, Z., Zhao, M., Liu, X., Lu, M., 2021. Speed control for SRM drive system based on switching variable proportional desaturation PI regulator. IEEE Access 9, 69735–69746.
Xiu, J., Wang, S., Xiu, Y., 2023. Optimum firing angles control for switched reluctance motor based on IPSO at steady state. IEEE Trans. Energy Convers.
Yang, F., et al., 2022. Improved direct torque control strategy for reducing torque ripple in switched reluctance motors. J. Power Electron. 22 (4), 603–613.
Zhang, X., Yang, Q., Ma, M., Lin, Z., Yang, S., 2019. A switched reluctance motor torque ripple reduction strategy with deadbeat current control and active thermal management. IEEE Trans. Veh. Technol. 69 (1), 317–327.